CHALMERS

Crack propagation analysis on the RM12 engine using real mission data

A prestudy for implementation in LTS

Master's thesis in Applied Mechanics

KNUT ANDREAS MEYER

Department of Applied Mechanics
Division of Materials and Computational Mechanics
CHALMERS UNIVERSITY OF TECHNOLOGY
Göteborg, Sweden 2014
Master's thesis 2014:14

MASTER'S THESIS IN APPLIED MECHANICS

Crack propagation analysis on the RM12 engine using real mission data

A prestudy for implementation in LTS

KNUT ANDREAS MEYER

Department of Applied Mechanics
Division of Materials and Computational Mechanics
CHALMERS UNIVERSITY OF TECHNOLOGY

Göteborg, Sweden 2014

Crack propagation analysis on the RM12 engine using real mission data
A prestudy for implementation in LTS
KNUT ANDREAS MEYER

Master's thesis 2014:14
ISSN 1652-8557
Department of Applied Mechanics
Division of Materials and Computational Mechanics
Chalmers University of Technology
SE-412 96 Göteborg
Sweden
Telephone: +46 (0)31-772 1000

Cover:
JAS39 Gripen

Chalmers Reproservice
Göteborg, Sweden 2014

Crack propagation analysis on the RM12 engine using real mission data
A prestudy for implementation in LTS
Master's thesis in Applied Mechanics
KNUT ANDREAS MEYER
Department of Applied Mechanics
Division of Materials and Computational Mechanics
Chalmers University of Technology

Abstract

GKN Aerospace Engine Systems have developed a life tracking system (LTS) to keep track of the life for each specimen of many components in the RM-12 engine in JAS39 Gripen. While the fan discs are currently analyzed with respect to crack initiation using LTS, the critical area in the connection between the fan discs and blades is not analyzed in LTS. Here, the dimensioning failure mode is crack propagation after initiation from fretting. This thesis aims to guide the implementation of the crack propagation failure mode in LTS, particularly for this critical connection. The current analysis is based upon a predefined mix of virtual missions aiming to represent the use of the aircraft. An implementation in LTS implies using logged data from each mission, yielding more accurate loading conditions.

The crack propagation analysis software NASGRO is used to analyze the crack growth for real mission data, thus only models available in this package have been evaluated. The chosen models are the Non-Interaction model based on the NASGRO-equation, which is a constant amplitude crack propagation model, and the Strip Yield model. Crack propagation material data has been fitted to both models, based on internal testing at GKN under the RAMGT test program. The Strip Yield model's applicability to crack cases with two fronts has been found to be limited, particularly due to insufficient documentation of the NASGRO implementation. Thus it is recommended to continue using the Non-Interaction NASGRO equation model. By analyzing 18 bulks of 500 missions each, the average mission had more than 25% longer life compared to the shortest life amongst these bulks. This indicates that the needed expense for inspection varies between different engines, and thus cost savings are possible. On the other hand, an analysis of the today used mix of virtual missions has revealed that it is non-conservative compared to the majority of missions. This is currently handled using safety factors. The importance of accounting for various factors have been analyzed, and based on this recommendations for improvements are given. These factors include, but are not limited to; ground missions (which is not included in the current analysis), missions missing from the LTS database (included in current analysis), stress field accuracy and equation parameters.

Keywords: NASGRO, Strip Yield, LTS, Crack propagation

Preface

This master thesis was written as the final stage of the Applied Mechanics master program at Chalmers University of Technology, ending my degree as "Civilingenjör" in Mechanical Engineering and MSc Applied Mechanics. It has been carried out at GKN Aerospace Engine Systems in Trollhättan. Magnus Andersson at GKN Aerospace Engine Systems has been supervising this project, and Lennart Josefsson at the Department of Applied Mechanics at Chalmers has been the examinator.

I would like to thank Magnus Andersson for the continuous support and help throughout the thesis. Lennart Josefsson has also earned my gratitude for contributing with his external views on the project and help finding relevant research. Furthermore, I would like to thank all the employees in the department for contributing to a welcoming working atmosphere, and always being eager to help out. A special thanks is given to Dr. Tomas Månsson, who has been the reference in crack propagation and helped guiding the direction of the study. Martin Carlsson and Niklas Gustavsson, writing their thesis simultaneously has also been great company and collaboration partners. Finally, my parents deserve huge thanks for their support throughout my entire education.

Knut Andreas Meyer
Trollhättan, Sweden 2014

Nomenclature

Abbrevations

CA	Constant Amplitude
CC	Corner Crack
GE	General Electric
LAS	Life Analysis System
LEFM	Linear Elastic Fracture Mechanics
LTS	Life Tracking System
NI	Non-Interaction (in this thesis NI model is equivalent to CA-model)
POD	Probability of detection
RAMGT	Robust aerofoils in modern gas turbines
RM12	Jet Engine in JAS 39 Gripen
SC	Surface Crack
SIF	Stress Intensity Factor (K)
SY	Strip Yield
VA	Variable Amplitude
VAC	Volvo Aero Coorperation

Symbols

a	Crack depth for 2D crack geometries (in thickness direction)	mm
c	Crack length for 2D crack geometries (in width direction)	mm
ΔK_{th}	Threshold SIF range	MPa$\sqrt{\mathrm{mm}}$
K_c	Critical SIF	MPa$\sqrt{\mathrm{mm}}$
K_{max}	Maximum SIF during cycle	MPa$\sqrt{\mathrm{mm}}$
K_{min}	Minimum SIF during cycle	MPa$\sqrt{\mathrm{mm}}$
K_{op}	Crack opening SIF	MPa$\sqrt{\mathrm{mm}}$
N	Number of cycles	Cycles
$\mathrm{NL_p}$	Number of partial cycles of low pressure shaft revolution speed	Cycles
NL	Revolution speed of low pressure turbine	rps
$\mathrm{NH_p}$	Number of partial cycles of high pressure shaft revolution speed	Cycles
NH	Revolution speed of high pressure turbine	rps
R	Stress ratio ($S_{\mathrm{max}}/S_{\mathrm{min}}$)	-
S	Nominal stress	MPa
t	Thickness of cracked body	mm
W	Width of cracked body	mm

Greek letters

α	Plane stress/strain tensile constraint factor	-
γ	Crack propagation test error measure	-
ρ	Crack plastic zone size	mm
σ_0	Flow stress	MPa
σ_y	Yield stress	MPa

Contents

1 Introduction

GKN Aerospace have developed and implemented a life tracking system (LTS) for RM12, the jet engine in JAS 39 Gripen. The system uses logged data from the airplanes as input for its life calculations. GKN claims that LTS yields a significantly higher accuracy than other jet engine manufacturers' equivalent systems [1].

The lives of the majority of the parts in RM12 are calculated towards crack initiation (CI) using a low cycle fatigue calculation based on the Coffin-Manson relation. When the calculations indicate that a component is close to crack initiation, the component is replaced even if no cracks are detected. The connection between discs and blades in the three fan stages are different, as CI is controlled by fretting for which GKN has no reliable prediction method. Due to this difficulty, the fan stages are inspected at a fixed interval of flight hours, based on a crack propagation analysis in NASGRO using a predefined mix of virtual missions.

By implementing crack propagation into LTS, each engine's inspection interval can be customized depending on the particular engine use. This may have a significant potential to optimize the inspection interval based on individual engine usage. The cost associated with each inspection is high, which drives this effort to adapt the inspection interval to each engine. From a crack propagation point of view, using logged data gives a possibility of taking load history effects into account. Elber [2] is one of several that has shown that single tensile overloads reduce crack growth rate for subsequent cycles. Such effects may increase the life of the components, as the current analysis is based on an Non-Interaction (constant amplitude) model. The term Non-Interaction implies that the load steps do not interact, thus the crack growth is independent of the residual stress state due to previous load steps.

Internal fatigue testing at GKN of the titanium alloys used in RM12 have revealed that some specimens may last an order of magnitude longer before crack initiation than other [3]. This indicates that some components which are replaced today, may have a significant amount of life remaining. Using crack propagation, a virtual crack, starting from the smallest detectable crack size, may be propagated using the continuously incoming data from flights. When the virtual crack has been propagated to a length were it is critical, the component can be called in for a new inspection. Thus a part does not need to be replaced before a crack has been discovered.

This thesis should serve as a pre-study for an implementation of a crack propagation model in LTS, in particular for the three fan stages. Should this method prove effective, crack propagation may also be implemented for more parts in RM12 which are replaced today based on calculated CI. The purpose and limitations of this thesis is more concisely described below.

1.1 Purpose

The purpose of this thesis is to:

1. Find a suitable method to analyze crack growth in the fan stages for RM12 spectrum loads.
2. Investigate how the crack growth in relation to flight hours vary between different individuals of the same component, as they may have been subjected to different usage.
3. Give recommendations for implementation of the crack propagation failure mode in LTS.

1.2 Limitations and assumptions

1. The stress field from GKN engine systems analysis along with the assumption that stresses are proportional to the fans rotational speed squared will be used. No new stress analysis will be performed.
2. For crack propagation analysis, NASGRO v7.01 will be used, as GKN Aerospace Engine Systems use this tool for all crack propagation analyses. Thus only models available in this software will be evaluated.
3. No new crack propagation tests will be performed, as that is out of budget for this thesis work.
4. The surface crack case SC02 will be used instead of the SC17 case currently employed by GKN, due to compatibility with the Strip Yield model.
5. Only the fan blades will be analyzed for real mission loads, as material tests are only available for the Ti 6-4 used here. It is assumed that similar trends are seen in the disc as it is subjected to the same load spectrum.

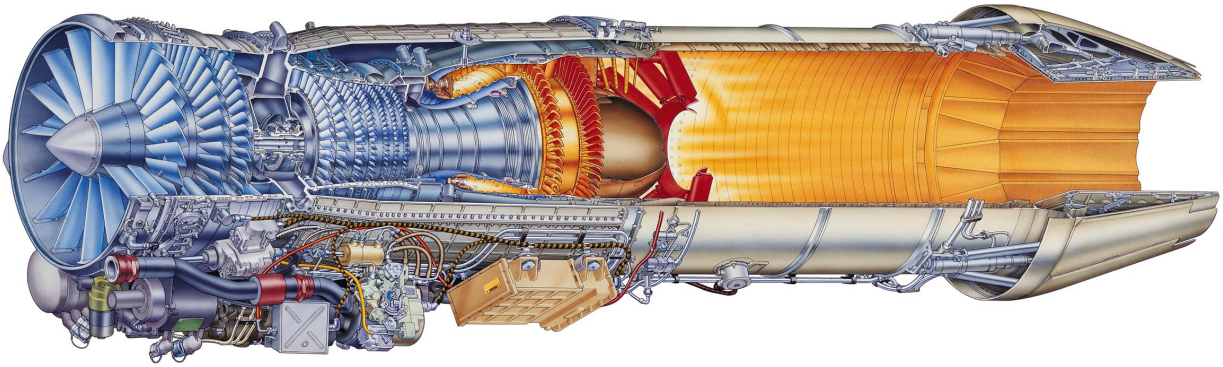

Figure 1.1: *The full RM12 jet engine*

1.3 RM12 engine overview

A picture of the full RM12 engine is given in figure 1.1. RM12 is a development of GE's F404, and has been modified to fit as a single engine in JAS 39 Gripen. The engine has a length of 4.04 m, a dry weight of approximately 1050 kg and maximum thrust about 80kN with afterburner [4]. Similar data, and more information on the RM12 engine is also given in [5]. The typical temperature after the fan stages, given 15°C inlet temperature, is 188°C. Further rearwards in the engine, temperatures can reach up to 1800°C. This thesis main focus is on the second fan disc stage. Due to the modest temperature gradients, GKN neglects thermal stresses in their calculations. This assumption reduce simulation times significantly as it permits the assumption of proportionality between revolution speed square and stress, as previously mentioned. The critical location for all the fan stages is the dovetail connection between the fan disc and the blades. Figure 1.2 gives a detailed view of this connection geometry, taken from the FE-model of fan stage 2.

1.4 Previous work

GKN's LTS system follows the life of all critical components in the different RM12 engines. For a general description of the LTS system, the reader is referred to the description given by Andersson [1]. This section will focus on the previous internal work at GKN on both the fan stages in RM12 and crack propagation analysis in general.

1.4.1 Current analysis of fan module

At the time of writing this thesis, each new individual of fan disc stage 2 and 3 are inspected for cracks after a certain amount of flight hours, and thereafter at an inspection interval one fifth of the initial amount of hours.

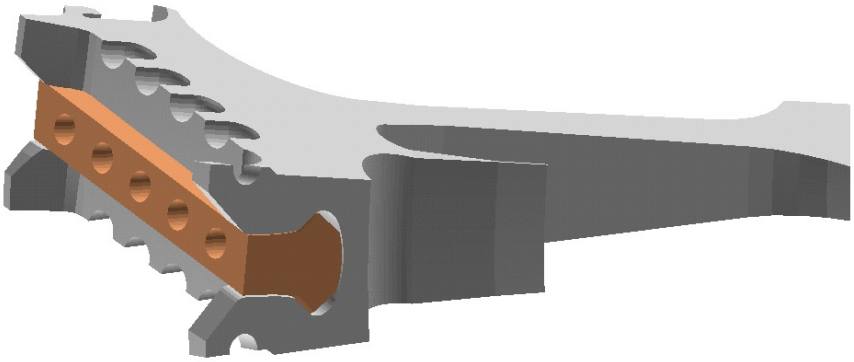

Figure 1.2: *Detailed view of dovetail connection between fan disc (grey) and bottom of blade (orange)*

The initial inspection interval is based on results from an experimental program [6]. The subsequent interval is, as previously mentioned, based on crack propagation analysis from detectable crack sizes to a critical crack sizes, such as in [7].

The start crack size in [7] had a depth 0.44 mm and width 1.44 mm for both surface and corner cracks in the blades and discs. A newer study of the probability of detection (POD) has revealed that the detectable crack size with 90% probability (95% confidence level) is significantly larger. A crack size of depth 0.63 mm for the disc [9] and 0.36 mm for the blade [10] has been found to give the previously mentioned desired POD. In these studies the depth to half-width ratio has been assumed to be 1 and only surface cracks were treated, i.e. semi-circular surface cracks. Compared to the disc, the cracks grow much slower in the blades. Therefore, the start crack analyzed in this thesis will be 0.63 mm in order to study the crack growth closer to the middle of the components crack propagation life. The critical crack depth of 1.5 mm used at GKN for the fan module in RM12 is based on previous experiments and analyzes.

The crack propagation analysis for the fan stages have been standardized by [11]. Here, stress gradients and maximum principal stresses from an elastic stress analysis of the contact between the disc and blade are used. The stress gradient consists of the maximum principal stress in all points throughout the thickness. The stress analysis [8] used by [7] has been performed at revolution speed 212.2 rps, and stresses are assumed to be proportional to the square of the rotational speed. For the blades, a critical location close to the center of the connection has been determined. This is given in figure 1.3a. For the disc, two critical locations have been

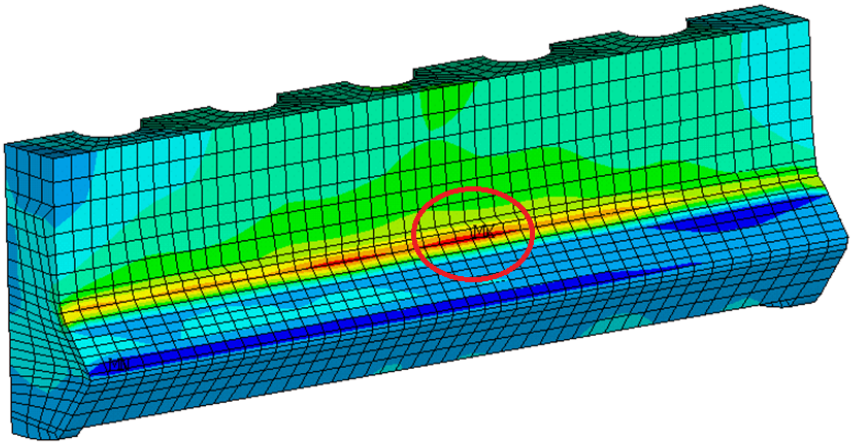

(a) *Critical location for blade, close to the center of the connection*

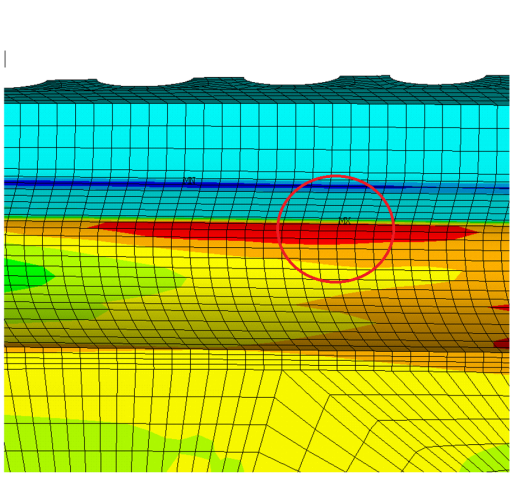

(b) *Critical location for the disc, close to the center of the connection*

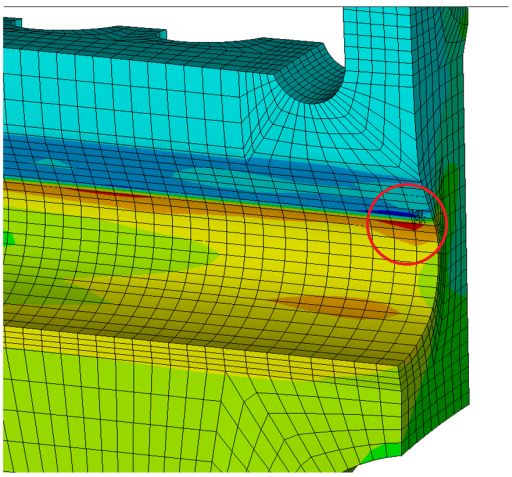

(c) *Critical location for the disc at the corner of the connection*

Figure 1.3: *Elastic stress solution for the dovetail connection between the disc and blade [8]. The critical locations are marked with red ellipses*

identified: Centrally in the connection (figure 1.3b) and at the corner of the connection (figure 1.3c).

These critical locations yield two different crack cases to consider; a surface crack and a corner crack. The cases chosen in NASGRO to model these are SC17 and CC09, which both accept a crack plane stress input, 1D and 2D respectively. The geometries for these crack cases are given in figure 1.4a and 1.4b respectively.

The input load data to the performed crack propagation analysis is predefined flights in the so-called A3B3 mix. This consists of a number of different virtual missions, and these are weighted by how often they are assumed to occur. The number of flight hours from start crack to critical crack is calculated for each of these, and the weighted average is taken as the number of flight hours before replacement is needed. The cycle counting is performed with standard rainflow counting technique, and a load cycle input file (longblock file) to NASGRO is created for each mission in the mix. The NASGRO analysis use the standard NASGRO equation with no load interaction, which is denoted consistent with NASGRO's notation as a Non-Interaction model (NI-model) is in this thesis. This model assumes constant amplitude (CA) loading and can therefore also be denoted as a constant amplitude model.

1.4.2 Crack propagation material calibration

Conventionally, material parameters for the NASGRO equation are fitted using least squares fit to $\mathrm{d}a/\mathrm{d}N$ versus ΔK data. This is done for a range of different values of the plane stress/strain constraint factor α, and the result giving the lowest standard deviation is chosen. This method is currently used for deriving data used in analyses at GKN. Rudenfors [13] proposed to use NASGRO simulation and an error estimate based on quality of prediction to determine which stress/strain constraint factor to be used. Here, a relation between the load parameter $S_{\max}/\sigma_0$ and α yielding no crack closure at a specified R-level has been used. The R-level was decided from visual inspection of crack growth rate curves; for what lowest R-ratios the difference between them is negligible. A number of combinations of the two parameters were tested in NASGRO, but no distinct minimum could be identified. The physicality of using α as a material parameter, can be debated since it, by definition, only depends on the geometry and Poisson's ratio. The values of α currently used by GKN when analyzing the RM12 engine varies significantly with temperature, which is not expected based on its definition.

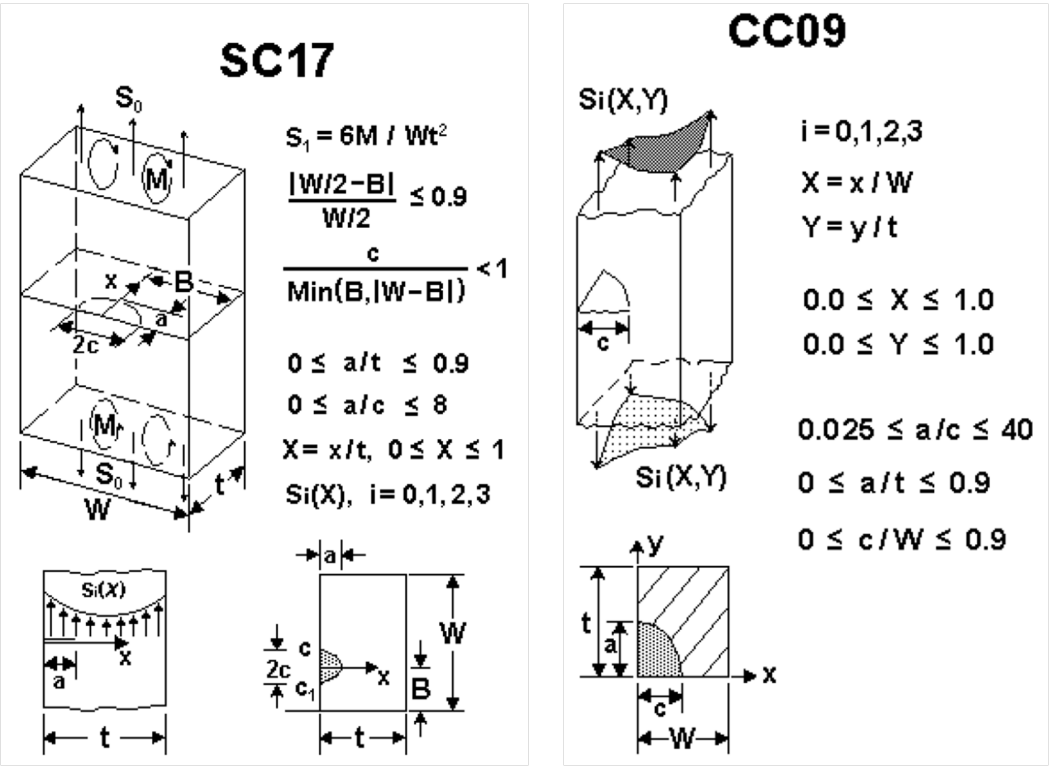

(a) *Surface Crack in NASGRO (SC17) [12]* (b) *Corner Crack in NASGRO (CC09) [12]*

Figure 1.4: *Crack geometries used for crack propagation in fan modules [7]*

At GKN, no material data has been fitted to any interaction models. Hansson and Månsson [14] and Rudenfors [15] have attempted using the Strip Yield model with material parameters calibrated for the NASGRO equation. For the same spectrum tests Hansson and Månsson's [14] calculations yielded nonconservative estimates, while Rudenfors [15] calculated only conservative estimates. Rudenfors [15] used a linear elastic estimation for stress for the strain controlled tests, which gives conservatively high stresses in the cases of significant plasticity, while the methodology used by [14] is not well described.

2 Theory

In this chapter some modern crack propagation models relevant for this master thesis are presented. The presentation is limited to models that are available within NASGRO, as this is the chosen analysis tool (see Limitations 1.2). The Non-Interaction models presented are the NASGRO and Walker equations. In NASGRO, five load interaction models are available: Generalized Willenborg, Modified Generalized Willenborg, Chang-Willenborg, Strip Yield and Constant Closure. Before describing the more advanced models available in NASGRO in detail, an overview of the basics of fracture mechanics is given.

2.1 Fracture mechanics basics

The stress intensity factor K is a measure of the stress state in vicinity of the crack, and depends on the loading, geometry and crack length. The region in which the stress intensity factor describes the state of stress is called the K-dominant zone. Here the elastic stress solution is proportional to $r^{-1/2}$, where r is the distance from the crack tip. Since real materials cannot withstand the infinite stress as $r \to 0$, a plastic zone develops close to the crack tip. When using the stress intensity factor as a measure of the crack severity, i.e. linear elastic fracture mechanics (LEFM), the effect of the plastic zone is neglected. For LEFM to be applicable, this plastic zone size must thus be small compared to the K-dominant zone. Downling [16] states that equation (2.1) must be satisfied for LEFM to be valid.

$$a, (b-a), h \geq \frac{4}{\pi}\left(\frac{K_{\max}}{\sigma_y}\right)^2 \tag{2.1}$$

Here a denotes the crack length, b the part width, h the part thickness and σ_y the material yield limit. This limitation is as [16] mentions fairly strict for fatigue crack growth, as it compares the dimensions of the monotonic plastic zone size to the other dimensions. Analyzing an elastic, perfectly plastic material, [16] shows that the cyclic plastic zone size can be approximated to one-fourth the size of the monotonic for a stress ratio of $R = 0$, thus indicating that the limitations on LEFM can be somewhat relaxed for cyclic loading, i.e. crack propagation.

In the 1960s Paris proposed a relation between fracture mechanics and fatigue crack growth known as Paris law (2.2).

$$\frac{\mathrm{d}a}{\mathrm{d}N} = C\Delta K^n \tag{2.2}$$

This power law has it applicability at medium stress intensities, as can be seen in stage II in figure 2.1. Here, a typical crack growth behavior for metals, based on the NASGRO equation (see section 2.2), has been

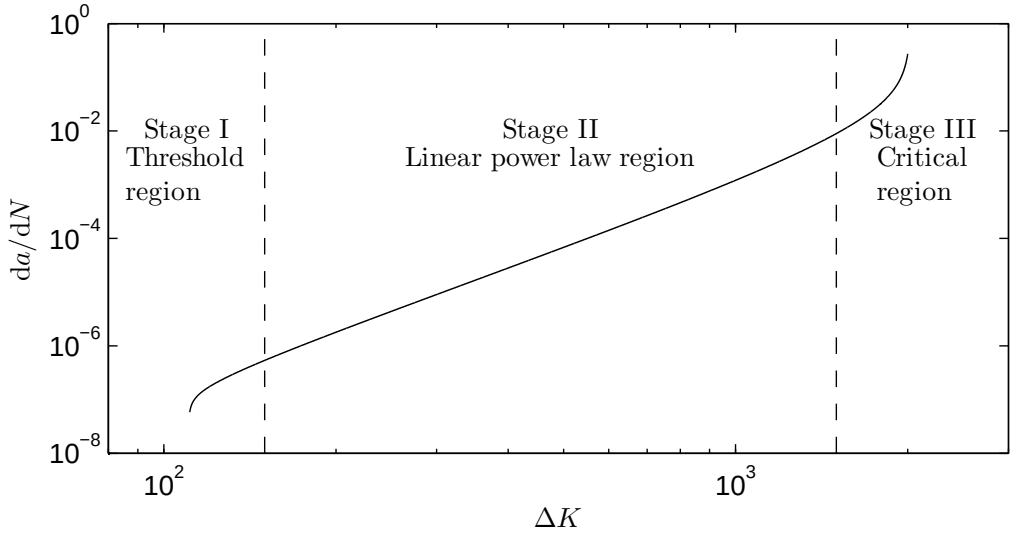

Figure 2.1: *Typical crack growth for metals*

plotted from ΔK values close to the threshold value up until values close to final fracture. The crack growth rate has proven to depend on the stress ratio as well as the stress intensity factor range, see for example [16, figure 11.11]. The more advanced models attempt to model this behavior as well as the crack growth in all stages in figure 2.1.

2.2 The NASGRO equation

The NASGRO equation (2.3), used by the crack propagation analysis software NASGRO is given in [12] as

$$\frac{\mathrm{d}a}{\mathrm{d}N} = C\left[\frac{1-f}{1-R}\Delta K\right]^n \frac{\left(1-\frac{\Delta K_{\mathrm{th}}}{\Delta K}\right)^p}{\left(1-\frac{K_{\max}}{K_c}\right)^q} \tag{2.3}$$

Here, a is the crack length, N the number of cycles, R is the stress ratio and C, n, p and q are empirically derived constants. f is the crack opening function, ΔK is the stress intensity range, ΔK_{th} is the threshold stress intensity range factor, $K_{\max}$ is the maximum stress intensity and K_c is the critical stress intensity factor. These parameters are described further in the following sections. The NASGRO equation offers two major improvements over the more simpler Paris power law. Firstly, it accounts for the crack opening stress through the crack opening function. By inserting $f = \frac{K_{\mathrm{op}}}{K_{\max}}$ and $R = \frac{K_{\min}}{K_{\max}}$ the first factor of the equation can be simplified as follows:

$$\left[\frac{1-f}{1-R}\Delta K\right] = \left[\frac{K_{\max}-K_{\mathrm{op}}}{K_{\max}-K_{\min}}(K_{\max}-K_{\min}\right] = K_{\max}-K_{\mathrm{op}} \tag{2.4}$$

This term is often denoted ΔK_{eff} and accounts for the growth rate dependence on the stress ratio R. Other methods for determining ΔK_{eff} has been proposed in the literature [17]. The last factor of the equation allows fitting of test data not only in the linear exponential growth region, but both near the threshold and for the accelerated growth towards the end of the component lifetime.

2.2.1 Crack opening function

The crack opening function f implemented in NASGRO is based on [18], and is defined according to

$$f = \frac{K_{\mathrm{op}}}{K_{\max}} = \begin{cases} \max(R,\ A_0 + A_1 R + A_2 R^2 + A_3 R^3) & R >= 0 \\ A_0 + A_1 R & -2 <= R < 0 \end{cases} \tag{2.5}$$

The empirical constants A_i used in NASGRO are derived from an analysis of center-cracked panels with constant amplitude loads. They are given as

$$A_0 = (0.825 - 0.34\alpha + 0.05\alpha^2)\left[\cos\left(\frac{\pi}{2}\frac{S_{\max}}{\sigma_0}\right)\right]^{\frac{1}{\alpha}} \tag{2.6}$$

$$A_1 = (0.415 - 0.071\alpha)\frac{S_{\max}}{\sigma_0} \tag{2.7}$$

$$A_2 = 1 - A_0 - A_1 - A_3 \tag{2.8}$$

$$A_3 = 2A_0 + A_1 - 1 \tag{2.9}$$

Here $S_{\max}/\sigma_0$ is the ratio of maximum applied stress to the flow stress. Most built in materials in NASGRO were curve fitted with a ratio of 0.3, as [12] claims this to be close to an average value obtained from fatigue crack growth tests using a variety of specimen types. The flow stress is the instantaneous stress level required for yielding. Newman [18] assumes this to be the average of the ultimate and yield stress. NASGRO uses this measure of flow stress to check for the full section yielding failure criteria. α is the plane stress/strain constraint factor, which theoretically is 1 for plane stress and 3 for plane strain. Newman [18] claims that adequate correlation of growth rates are achieved by using the constraint factor as a fitting parameter. However, due to the plastic zone varying with the size of ΔK (or more specifically with K_{max}), he also claims that better correlation can be achieved by allowing α to vary with ΔK.

2.2.2 Stress intensity factor

The stress intensity factor range is given as $\Delta K = K_{\max} - K_{\min}$ [16]. In the NASGRO software K is calculated for cracked bodies under combined loading according to equation (2.10) [12].

$$K = [S_0F_0 + S_1F_1 + S_2F_2 + S_3F_3 + S_4F_4]\sqrt{\pi a} \tag{2.10}$$

Here S_i is a reference stress for different loading conditions, such as pure tension or bending. F_i is the corresponding geometric correction function, which depends on the loading type and geometry. $K_{\max}$ is the stress intensity corresponding to the peak load in the current cycle, and $K_{\min}$ is defined equivalently. For some more advanced crack cases in NASGRO, it is possible to analyze crack growth with a user specified stress field. This is possible with the use of so called weight functions. As noted by [19] a SIF solution for one set of boundary conditions contains sufficient information to solve another SIF for different boundary conditions. The result of the analysis in [19] is that the stress intensity factor can be described according to equation (2.11). Here $h(x)$ is the weight function that depends on the geometry only, $p(x)$ is the uncracked crack plane stress and Γ_c is the crack perimeter.

$$K = \int_{\Gamma_c} p(x)h(x)\mathrm{d}x \tag{2.11}$$

2.2.3 Threshold stress intensity range factor

NASGRO implements two different approximations of the threshold stress intensity factor depending on the stress ratio R, these are given in equations (2.12) and (2.13).

$$\Delta K_{\text{th}} = \Delta K_1^* \frac{\left[\frac{1-R}{1-f[R]}\right]^{1+RC_{\text{th}}^p}}{(1-A_0)^{(1-R)C_{\text{th}}^p}} \quad R \geq 0 \tag{2.12}$$

$$\Delta K_{\text{th}} = \Delta K_1^* \frac{\left[\frac{1-R}{1-f[R]}\right]^{1+RC_{\text{th}}^m}}{(1-A_0)^{C_{\text{th}}^p - RC_{\text{th}}^m}} \quad R < 0 \tag{2.13}$$

Here $\Delta K_1^* = \Delta K_1\sqrt{a/(a+a_0)}$ where ΔK_1 is the threshold stress intensity factor range as $R \to 1$ and a_0 is a small crack parameter, typically $a_0 = 0.0015$inch (0.0381mm). This value is only effective when a is small. C_{th} is an emperical fitting parameter with different values for positive (superscript p) and negative (superscript m) R values. For Non-Interaction models in NASGRO there is an option to set $C_{\text{th}} = 0$, which yields low threshold stress intensity range factors and is thus the conservative choice. For interaction models $C_{\text{th}} = 0$.

2.2.4 Critical stress intensity factor

K_c is the stress intensity factor at which failure will occur through fracture. Increasing the thickness will, by approaching plane strain conditions, yield a K_c value approaching the commonly tabulated worst case plane strain value K_{Ic}. The NASGRO software use a generalization of a relationship proposed by G. A. Vroman in 1983, given in (2.14), to account for the effect of thickness on K_c.

$$\frac{K_c}{K_{\text{Ic}}} = 1 + B_k\mathrm{e}^{-\left(A_k\frac{t}{t_0}\right)^2}, \quad t_0 = 2.5\frac{K_{\text{Ic}}}{\sigma_{\text{ys}}} \tag{2.14}$$

Letting $A_k = B_k = 0$ implies neglecting the increased critical stress intensity factor for conditions approaching plane stress. Currently, all of GKN's material data conservatively assume plane strain conditions for the critical stress intensity factor.

2.3 The Walker equation

The standard Walker equation as presented in [16] is given as

$$\frac{\mathrm{d}a}{\mathrm{d}N} = C_0\left[\frac{\Delta K}{(1-R)^{1-\gamma}}\right]^m \tag{2.15}$$

Compared to the Paris equation (2.2), the walker equation includes an additional material parameter γ which controls the stress ratio sensitivity. γ does in general differ for $R \geq 0$ and $R < 0$, and for many materials (see [16, table 11.2]) it is set to zero for $R < 0$ which implies $\mathrm{d}a/\mathrm{d}N = C_0[K_{\max}]^m$. Thus the compressive portion of the loading is assumed not to contribute to crack growth. The implemented method in NASGRO differs from the equation presented in [16], as it has been modified by J. B. Chang for negative stress ratios [12], and have included positive and negative cutoff values for stress ratios, equation (2.16).

For $\Delta K > \Delta K_{\mathrm{th}},\ R \geq 0$

$$\frac{\mathrm{d}a}{\mathrm{d}N} = C\left[\frac{\Delta K}{\left(1-\bar{R}\right)^{1-m}}\right]^n, \qquad \bar{R} = \begin{cases} R, & R < R^+_{\mathrm{cut}} \\ R^+_{\mathrm{cut}}, & R > R^+_{\mathrm{cut}} \end{cases} \tag{2.16a}$$

For $\Delta K > \Delta K_{\mathrm{th}},\ R < 0$

$$\frac{\mathrm{d}a}{\mathrm{d}N} = C\left[\left(1+\bar{R}^2\right)^q K_{\max}\right]^n, \qquad \bar{R} = \begin{cases} R, & R > R^-_{\mathrm{cut}} \\ R^-_{\mathrm{cut}}, & R < R^-_{\mathrm{cut}} \end{cases} \tag{2.16b}$$

For $\Delta K < \Delta K_{\mathrm{th}}$

$$\frac{\mathrm{d}a}{\mathrm{d}N} = 0 \tag{2.16c}$$

The walker model does not inherently model more than the linear region (Stage II in figure 2.1), but the implementation in NASGRO allows the user to specify multiple material parameters such that the crack growth can be modeled by multiple linear segments in the logarithmic $\mathrm{d}a/\mathrm{d}N$ versus ΔK plot.

2.4 Generalized Willenborg model

The retardation effect in the Willenborg model is modeled by a residual SIF, based on residual compressive stresses ahead of the crack tip. The generalized Willenborg model used in NASGRO is an improvement over the original Willenborg model, as it predicts the observed phenomenon of crack arrest after a significant overload. The generalized model, cannot either predict a reduction in retardation due to an underload, or account for the effect of multiple overloads.

The effect of the overload is modeled as a change in stress ratio, so the Willenborg models only gives retardation when models that has a stress ratio dependence are used, such as the NASGRO or Walker equation. In NASGRO the NASGRO equation is used for the Willenborg models. An effective stress ratio is defined according to equation (2.17):

$$R_{\mathrm{eff}} = \frac{K_{\min} - K_R}{K_{\max} - K_R} = \frac{K_{\min,\mathrm{eff}}}{K_{\max,\mathrm{eff}}} \tag{2.17}$$

The residual SIF, K_R is calculated according to equation (2.18) in NASGRO.

$$K^W_R = K^{\mathrm{OL}}_{\max}\left(1 - \frac{\Delta a}{Z_{\mathrm{OL}}}\right)^{1/2} \tag{2.18a}$$

$$Z_{\mathrm{OL}} = \frac{\pi}{8}\left(\frac{K_{\max}}{\alpha_g \sigma_{\mathrm{ys}}}\right)^2 \tag{2.18b}$$

$$\alpha_g = \begin{cases} 1.15 + 1.4\mathrm{e}^{-0.95\left(\frac{K_{\max}}{\sigma_{\mathrm{ys}}\sqrt{t}}\right)^{1.5}}, & \text{1D Crack Case} \\ 1.15, & \text{2D Crack Propagation at free surface (plane stress)} \\ 2.55, & \text{2D Crack Propagation inside part (plane strain)} \end{cases} \tag{2.18c}$$

$$K_R = \phi K^W_R = \left[\frac{1 - \frac{\Delta K_{\mathrm{th}}}{\Delta K}}{R_{\mathrm{SO}} - 1}\right] K^W_R \tag{2.18d}$$

Here, $K^{\mathrm{OL}}_{\max}$ is the maximum SIF from the overload cycle. Δa is the distance the crack has grown since the last overload cycle and Z_{OL} is the size of the plastic zone created from the last overload cycle. α_g is a plane stress/strain constraint factor, modifying the size of the plastic zone. In the original Willenborg model, K^W_R was used as K_R, but to better predict crack arrest the modification in equation (2.18d) has been introduced. When $K^{\mathrm{OL}}_{\max}/K_{\max} > R_{\mathrm{SO}}$, $K_{\max}$ is forced to be $\Delta K_{\mathrm{th}}/(1-R)$ and the crack growth is arrested.

2.5 Modified Generalized Willenborg model

The modified generalized Willenborg model implemented in NASGRO has two changes compared to the generalized Willenborg model described above. The major advantage of these modifications is that reduction in growth retardation due to both compressive and tensile underloads is accounted for. In equations (2.18) the definition of the effective SIFs has been changed slightly, and the parameter ϕ in equation (2.18d) varies with the underload stress ratio, $R_{\mathrm{U}} = K_{\mathrm{UL}}/K_{\mathrm{max}}^{\mathrm{OL}}$, see equations (2.19).

$$K_{\mathrm{max}}^{\mathrm{eff}} = K_{\mathrm{max}} - K_R \tag{2.19a}$$

$$K_{\mathrm{min}}^{\mathrm{eff}} = \begin{cases} \max\left\{(K_{\mathrm{min}} - K_R),\ 0\right\}, & K_{\mathrm{min}} > 0 \\ K_{\mathrm{min}}, & K_{\mathrm{min}} \leq 0 \end{cases} \tag{2.19b}$$

$$\phi = \begin{cases} \min\left\{1,\ \frac{2.523\phi_0}{1.0+3.5(0.25-R_U)^{0.6}}\right\}, & R_U < 0.25 \\ 1.0, & R_U > 0.25 \end{cases} \tag{2.19c}$$

2.6 Chang-Willenborg model

The Chang-Willenborg interaction model implemented in NASGRO is equal to the Generalized Willenborg model, except that the Walker equation is used instead of the NASGRO equation. The equations are defined in section 2.3, and the only difference to the presented Walker relation is that the effective stress ratio, R_{eff}, defined in equation (2.17), is used.

2.7 Strip Yield model

In this report the Strip Yield model will refer to the modified Strip Yield model, which leaves plastically deformed material in the crack wake. First, the original Strip Yield model, as proposed by Dugdale [20], is described. Then, details of the modified Strip Yield model implemented in NASGRO, which deals with crack growth, is given.

2.7.1 Original Strip Yield model

The original Strip Yield model considered monotonic loading on a thin, infinite plate with a central through crack. The material was assumed to be linear, perfectly plastic and the plastic zone to be a thin strip under plane stress conditions. An effective crack length of $2a + 2\rho$, where $2a$ is the length of the central crack in the plate, and ρ is the length of the plastic zone, can be assumed. The size of the plastic zone is calculated so that the closure stress intensity factor cancels out the remote stress intensity factor. Andersson [19] shows that for these original assumptions, the plastic zone size can be calculated according to equation (2.20).

$$\frac{a}{a+\rho} = \cos\left(\frac{\pi\sigma}{2\sigma_y}\right) \tag{2.20}$$

To estimate an effective SIF, one could use $a_{\mathrm{eff}} = a + \rho$ as noted above, but this assumption tends to overestimate K_{eff} according to Andersson [19]. He proposes that another expression; equation (2.21), yields a more realistic estimate of the effective SIF. The derivation of this expression is also given in [19].

$$K_{\mathrm{eff}} = \sigma_y\sqrt{\pi a}\left[\frac{8}{\pi^2}\ln\left(\sec\left(\frac{\pi\sigma}{2\sigma_y}\right)\right)\right]^{\frac{1}{2}} \tag{2.21}$$

Using the relation (2.21) to plot the effective SIF, normalized by $\sigma_y\sqrt{\pi a}$, it is clear that as the nominal stress increases LEFM becomes nonconservative in the approximation of the severity of the SIF, see figure 2.2. In the same figure, the more simple Irwin correction, based on a pure force equilibrium for the redistribution of elastic to plastic stresses, has also been plotted. Unlike the Strip Yield correction, the Irwin correction does not predict an infinite SIF when $\sigma \to \sigma_y$. It does however give similar correction for $\sigma \leq 0.8\sigma_y$. A more detailed description of the Irwin correction is given in [19].

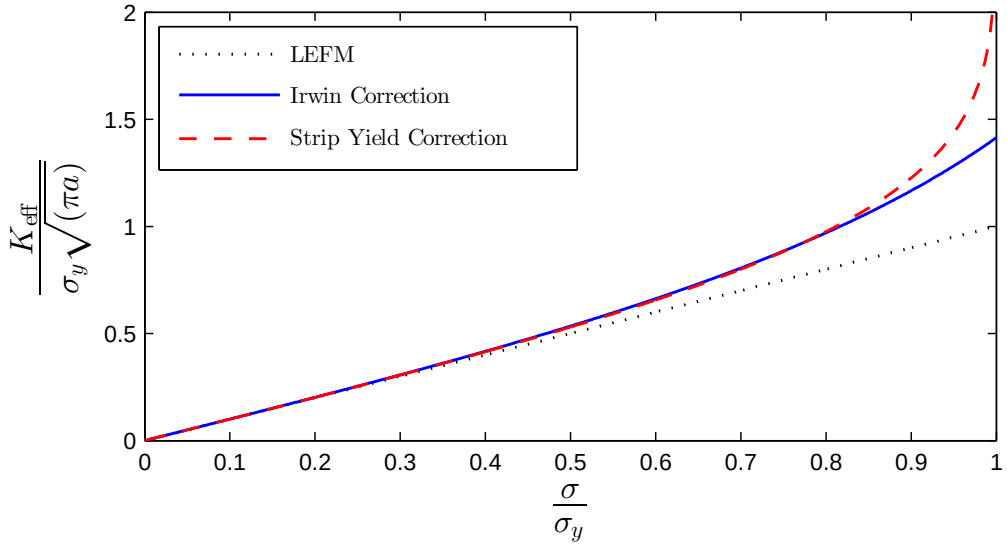

Figure 2.2: *LEFM Plasticity Corrections*

2.7.2 Modified Strip Yield model

When used to model crack growth, and particularly crack tip history effects, the original Strip Yield model is modified to leave plastically deformed material in the crack wake. This means that material that has been extended due to plastic deformation before rupture will cause the crack to close prematurely. Material surrounding the crack will thus have a residual stress which will prevent the crack from opening again, until the remote stress is great enough to overcome the residual stress. The SIF required to open the crack (i.e. no contact between ruptured crack faces) is K_{op} and the corresponding stress S_{op}. The effective SIF range can then be calculated as $\Delta K_{\text{eff}} = K_{\max} - \max\{K_{\text{op}},\ K_{\min}\}$. If sufficiently large compressive stress is applied to the crack surface, the ruptured parts may yield in compression and thereby reduce the crack closure level. This phenomenon is modeled by a finite set of perfectly plastic bars along the crack centerline. Crack growth is accomplished by releasing an appropriate number of these bars. The most famous implementations of the Strip Yield model, according to [21], are Newmans constant constraint loss model [22] and De Koning's variable constraint loss model, both should be available within NASGRO [12]. However, GKN only have access to Newman's constant constraint option.

The models differ in the way they handle the tri-axial stress states due to more complex crack geometries than a through crack in an thin and wide plate. This becomes particularly important for three dimensional crack geometries, such as a surface or corner crack. Newman [22] introduced the plane stress/strain constraint factor α to account for the tri-axial stress state, and both models use this concept. The background for α is that for a tri-axial stress state that occurs in plane strain conditions, the material can sustain higher maximum principal stress before yielding than during a bi-axial tensile stress state in plane stress conditions. For $\nu = 1/3$, using Trescas yield criterion, it can be showed that $\alpha = \sigma_1/\sigma_{\text{eff}} = 1$ for plane stress and $\alpha = 3$ for plane strain for the stress field in front of a crack along the crack centerline.

Newman's constant constraint loss model assumes that α is constant along the elements of the plastic zone. The value will, however, depend on the state of stress. This is based on the empirical observation that cracks start to grow perpendicular to the loading direction (plane strain), but towards the end of the life an inclined crack plane can be observed. Newman proposed that the transition occurs when the cyclic plastic zone reaches a certain percentage of the specimen thickness [12], see equation (2.22) where $(\Delta K_{\text{eff}})_T$ denotes the transition effective SIF, μ is proportionality coefficient and B is the specimen thickness.

$$(\Delta K_{\text{eff}})_T = \mu\sigma_0\sqrt{B} \tag{2.22}$$

According to [12], Newman found that $\mu = 0.5$ was suitable for thin sheets and a range of materials within a scatter band of $\pm 20\%$. A general trend was lower values for thicker specimens. The constraint value changes linearly from the plane strain user set value, to the plain stress value of $\alpha = 1.2$ which is fixed, over one decade of crack growth rate. The transition starts when $\Delta K_{\text{eff}} = (\Delta K_{\text{eff}})_T$. According to [12] this transition region is not well understood and is subject to further research. The constraint factor for compressive yielding is always

set to 1. This description of the implementation is based on the NASGRO main reference manual [12]. The behavior of the program is not always consistent with this description, this is discussed in appendix A.

2.8 Constant Closure model

The Constant Closure model is a simplified closure model that uses the observed phenomenon that for some spectra the crack closure level is fairly stable around some level. For this to occur the load spectra should contain controlling over and underloads which occur often enough to keep residual stresses in the crack wake, thus maintaining a constant opening stress [12]. There are different ways of determining the closure levels: Direct user entry, empirical fit to different spectra with a stress ratio representative of the spectrum (R_{spec}) or using Newmans crack closure function from the standard NASGRO equation on R_{spec}.

3 Method

As given in section 1.1, this thesis have three main objectives: (1) Finding a suitable method to analyze crack growth in the fan in RM12, (2) investigating how the crack growth varies for different individuals of the same component, due to different usage and (3) giving recommendations for implementation of crack propagation in LTS. The methodology followed in the thesis is given below:

1. Through a literature survey of the different crack propagation models available in NASGRO v7.01, find the most suitable model for analyzing the given load cases.
2. Fit CA amplitude test data to the chosen model(s).
3. Compare results of model(s) to a RM12 spectrum crack propagation test.
4. Evaluate effect of different cycle counting techniques and if the choice of this has an significant impact on the results.
5. Evaluate if the contribution to crack growth from ground and missing missions needs to be accounted for.
6. Using the chosen method; analyze a set of different individuals and investigate how the life differs between these.
7. Investigate the importance of some parameters on crack growth in order to give recommendations on what parts of the analysis needs improvement.

3.1 Choice of Crack Propagation models

A model for simulating the crack growth in the fan should be able to account for a complicated stress history, as well as compensate for violation of the small scale yielding criterion (equation 2.1). The NASGRO equation (2.3) has the latter effect incorporated in Newman's crack opening function in which $S_{\max}/\sigma_0$ is included. With this method the user has to specify a fixed load level to use throughout the spectrum. The NASGRO equation is not an interaction model, thus no history effect is accounted for. The available interaction models in NASGRO are, as described in the theory section:

1. Generalized Willenborg model
2. Modified Generalized Willenborg model
3. Chang-Willenborg model
4. Strip Yield model
5. Constant Closure model

Khan et al. [21] categorizes interaction models into three different categories, depending on the underlying phenomena they utilize to model the interaction effect: Yield zone models, crack closure models and Strip Yield models. Only the constant closure model in NASGRO can be considered a crack closure model, but this is not a true interaction model as it requires preset values to describe the spectrum. As this model assumes that the closure level reaches a constant value, it could be an applicable model if fast simulation times are a requirement, and more advanced models have proven that the variation of closure level throughout the spectrum is limited. The Willenborg models (nr. 1-3 above) are categorized as yield zone models, as these models the interaction effects as functions of the yield zone ahead of the crack tip. Crack retardation is, however, more commonly attributed to residual plastic deformations in the crack wake, causing premature crack closure. This effect is modeled by both crack closure models and Strip Yield models. Khan [21] have evaluated different interaction models based on a literature study. He use the models ability to predict the effect of the following load situations to evaluate the models:

1. Single overload
2. Multiple overloads

3. Overload interaction
4. Single underload
5. Multiple underloads
6. Delayed retardation
7. Crack acceleration
8. Crack arrest
9. Effect of thickness

The Generalized Willenborg model can only handle single overloads, and not multiple overloads, underloads, overload interactions or delayed retardation. It does, however, predict crack arrest based on the ratio of the overload SIF and the subsequent SIF. Crack acceleration is not predicted. The effect of thickness is considered through the plane stress/strain constraint factor from a special fit [12]. In addition this model does not have a correction for crack tip plasticity. The modified generalized Willenborg model improves the unmodified by incorporating the effect of single underloads by reducing the retardation effects. It does not, however, predict acceleration of crack growth. The Chang-Willenborg model has similar properties to the modified generalized Willenborg, except that the underlying crack growth relation is the Walker relation. According to [21] the Strip Yield models predicts all of the above phenomenon except the effect of thickness. This is incorporated in the constant constraint loss option used by GKN, but [21] claims that the thickness effect modeled by the constraint factor is poor. Even though Khan [21] concludes that the Strip Yield model is the best model for simulating spectrum loading (as of 2007), he claims that its applicability is, as most other models, limited to 2-dimensional crack cases. This statement is strengthened by the findings by [23], that showed that the constraint factor may not be enough to give good predictions for both CA and VA loading. The conclusion that the single value for the constraint factor may not be sufficient to describe all R-ratio and interaction effect, indicates that it cannot be expected to model the thickness behavior correctly.

Even though the Strip Yield model in NASGRO has some limitations, particularly for the 3D crack geometries treated in this thesis, it is the best available method within NASGRO, and perhaps in all commercial software [21] as of 2007. Skorupa [23] found that the variable constraint loss option was better than the constant constraint option available in GKN's version of NASGRO. Due to the limitations (see section 1.2) the variable constraint loss option is not studied further. For future work it could be worthwhile evaluating if this model would be better suited for modeling spectrum loading. The Strip Yield model with the constant constraint loss option will be the method of choice for analyzing the spectrum loading. The Non-Interaction NASGRO equation will also be used. The purpose of using the Non-Interaction NASGRO equation in addition is to compare with the more advanced Strip Yield model, and to have the reference as the currently used model.

3.2 Material data calibration

Material parameters are calibrated for both the Non-Interaction NASGRO equation and the Strip Yield model. The NASGRO manual [12] instructs the user to use α as a fitting parameter while analyzing constant amplitude tests with the Strip Yield model. An equivalent approach is used to fit the Non-Interaction model, similar to the model proposed by Rudenfors [13]. GKN has performed three crack propagation tests on an RM12 simulated mission, at different load levels. From these, the elastic, load controlled, test will be used to evaluate how well the models predict the life of a spectrum loading situation. Noting that this is not sufficient data to determine how accurate the models are, it will only give an indication on their applicability.

3.2.1 Crack propagation testing

In this section, the details of the tests that form the basis of the material data calibration in this thesis will be given. Although this is not work performed by the author, it is considered important to give a more detailed overview of this work as the results are analyzed directly. The two tests performed both tested so-called "Kb-specimens" which are the standard test specimen at GKN, as these are considered to be more similar to real parts than the simple 2D geometries often used in research, such as in [24]. The test specimen specifications are standardized at GKN according to figure 3.1.

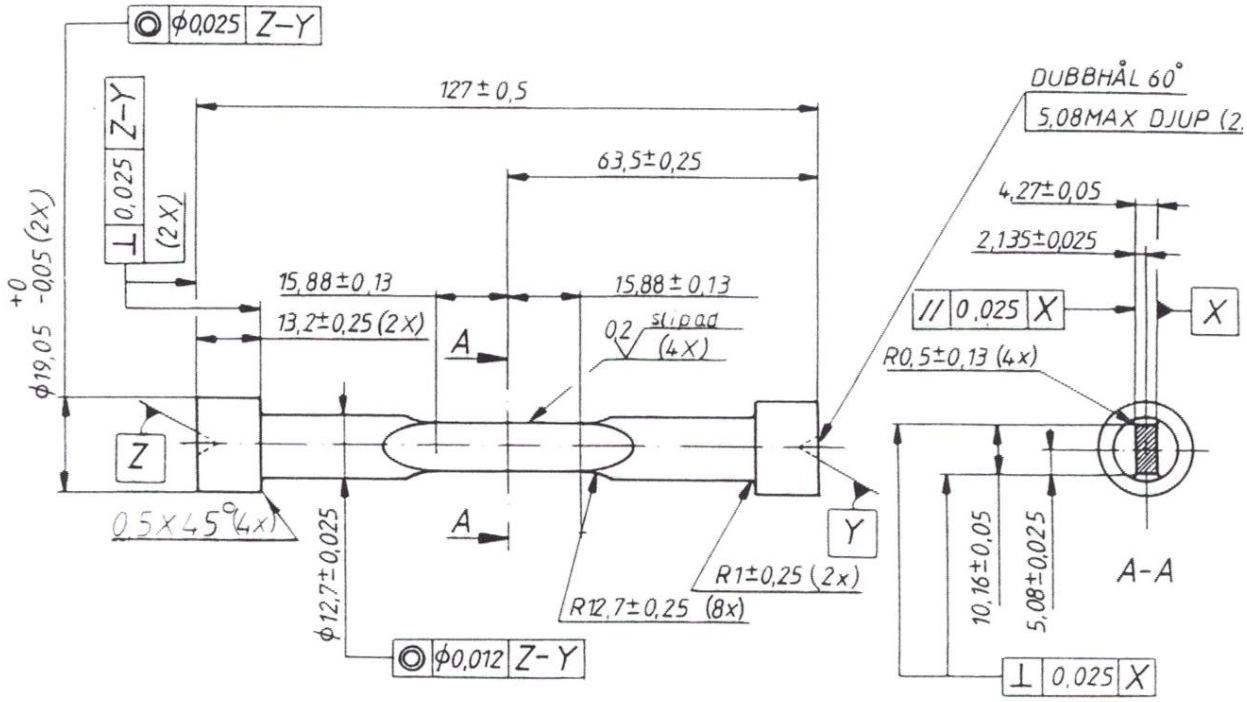

Figure 3.1: *Standard Kb specimen dimensions used at GKN [25]*

For this test specimen, the simple surface crack case SC01 in NASGRO is appropriate, and is used at GKN for this test specimen, see for example [15]. The geometry and other details of this crack case is given in figure 3.2. It can be noted that this crack case is very similar to SC17 and SC02 used to analyze the critical location in the blade. The differences are that a non-uniform stress field can be applied, and, in the SC17 case, the crack doesn't need to be centered.

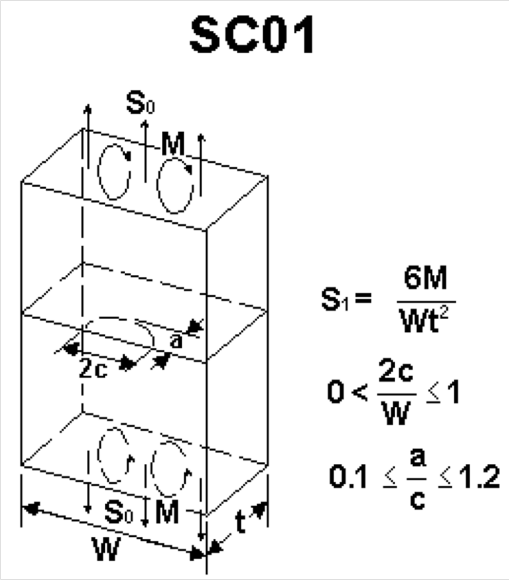

Figure 3.2: *Crack case "SC01" in NASGRO [12]*

Table 3.1: Overview of CA tests performed in the RAMGT test program ("N_{dp}" denotes number of recorded datapoints and "Th?" if the test is a threshold test or not)

Test specimen	**R**	$\mathbf{S}_{max}$[MPa]	**w**[mm]	**t**[mm]	**Th?**	$\mathbf{N}_{dp}$	$\mathbf{a}_{start}$[mm]	$\mathbf{a}_{end}$[mm]
FPV10490-1191-19	0.8	414	10.19	4.29	yes	77	0.7050	1.4650
FPV10490-1191-13	0.8	765	10.17	4.30	no	161	0.3250	1.9250
FPV10490-1191-7	0.8	765	10.17	4.29	no	163	0.3050	1.9250
FPV10490-1191-17	0.6	239	10.19	4.29	yes	110	0.6850	1.7750
FPV10490-1191-11	0.6	630	10.18	4.30	no	191	0.4450	2.3450
FPV10490-1191-4	0.6	605	10.19	4.29	no	212	0.2350	2.3450
FPV10490-1191-18-10	0.3	182	10.19	4.30	yes	92	0.6750	1.5850
FPV10490-1191-18-18	0.3	182	10.19	4.30	yes	21	1.6750	1.8750
FPV10490-1191-14	0.3	550	10.18	4.30	no	227	0.2850	2.5450
FPV10490-1191-8	0.3	550	10.20	4.29	no	200	0.2950	2.2850
FPV10490-1191-3	0.3	550	10.19	4.29	no	107	1.2850	2.3450
FPV10490-1191-16-13	0.0	163	10.17	4.30	yes	14	0.6950	0.8250
FPV10490-1191-16-15	0.0	157	10.17	4.30	yes	120	0.9150	2.1050
FPV10490-1191-12	0.0	550	10.19	4.30	no	225	0.2750	2.5150
FPV10490-1191-2	0.0	550	10.20	4.30	no	93	0.4355	1.8590
FPV10490-1191-9	-1.0	500	10.18	4.30	no	220	0.3550	2.5850
FPV10490-1191-6	-1.0	500	10.17	4.30	no	196	0.3350	2.2850

Constant amplitude testing

Constant amplitude testing has been performed within the EU test program RAMGT (Robust aerofoils in modern gas turbines), in which Volvo Aero Cooperation (VAC) participated in 2003. An advantage of this test data compared to standard test data at GKN is more stress ratios, five instead of three. Furthermore, spectrum testing (see next section) has been performed on test specimens from the same batch, that was not used in the RAMGT program [26]. An overview of the CA test specimens is given in table 3.1.

RM12 spectrum testing

As a follow up after the RAMGT test program, VAC tested crack propagation in specimens subjected to spectrum loading at different load levels. For Ti 6-4 three specimens where tested, but only one at load levels for which linear fracture mechanics is valid and comparable to load levels in real missions. From these tests, only raw data in addition to start and end crack conditions are available. The crack size has been monitored by the dc potential drop technique. In order to translate this signal into a crack length, an electric FE analysis has been carried out (figure 3.3). Due to unavailability of documentation from the testing, the probe locations have been taken from the standard test specification [27]. The notch size has been taken from RAMGT data, but the double notch size has also been analyzed to see how big impact this has on the result. The test started at a crack depth of $a = 0.64$ mm and ended at $a = 2.65$ mm, and the FE-analysis has been performed for 11 equally

(a) *Boundary conditions* (b) *Test sample mesh* (c) *Crack initiation notch*

Figure 3.3: *FE-analysis of potential drop measurements*

spaced values within this interval. The crack shape is assumed to be semicircular throughout the test, which is confirmed through visual inspection by [15]. The notch is illustrated in figure 3.3c, and the full mesh of the test sample is given in figure 3.3b. Current flow is applied to the back face of the sample, and the symmetric test sample allows to set zero voltage on the uncracked surface (figure 3.3a). The model is further simplified by employing symmetry along the sample, analyzing only half the crack.

Since the exact current (I) used in the test is unknown, as well as the resistivity of the particular titanium alloy (r), the results from the simulation needs to be scaled to get a function translating the measured potential drop value to a crack length. Assuming that the resistance of the structure only depends on the material and geometry, the potential drop V can be calculated as $V(a) = Irf(a)$ where $f(a)$ describes the geometry as a function of a. The desired outcome should be a function $a = g(V)$, which is given as $g(V) = f^{-1}(V/Ir)$. As Ir is not the same in the test and in the experiment, the simulated values of V are linearly scaled and shifted, to match the test values at the start and end point. This works as the start and end simulated crack lengths are equal to those of the experiment.

3.2.2 Non-Interaction model

The difference between the earlier proposed method [13] and the current, is the treatment of the load parameter $S_{\max}/\sigma_0$ in Newman's crack opening function (equation (2.5)). Earlier, this was kept at a constant value for all tests, but the current method varies this to fit the load level of the particular test. One advantage of this methodology is the possibility to adjust this parameter to the real operating loads, which may differ from those of the test. This load parameter may be difficult to define in real cases for two main reasons. Firstly, the nominal stress can be hard to define for complex geometries and crack cases. Secondly, in VA loading conditions this parameter varies between cycles, which is not possible in NASGRO which means that a fixed value has to be chosen.

3.2.3 Strip Yield model

The fitting procedure for the Strip Yield model proposed by the NASGRO manual [12], is not considered sufficient according to [23, 24]. The arguing for this is that the crack interaction effects are far more sensitive to the constraint factor than the R-dependence, thus decent curve fits can be achieved for a range of values for α. For this reason, additional experiments with single spike overloads and other VA loading conditions should be conducted to derive better values for the constraint factors [24]. At the writing of this thesis, GKN does not have these types of tests. Therefore, a method similar to the one recommended by the NASGRO manual will be employed. Using the same material data fitting procedure as for the Non-Interaction model above, the material parameters C, n, p and q will be fitted for a range of α values. These α values are denoted α_{mp} as they control the other material parameters. For each α_{mp}, simulations of the constant amplitude tests will be performed for a range of α values. These α values are denoted α_{SY} as these are the actual tensile yield constraint factors supplied to NASGRO. This creates a two dimensional dataset of error values for the simulations, from which the combination of material parameters (α_{mp}) and tensile yield constraint factor (α_{SY}) yielding the lowest errors can be selected. By choosing this method it should be noted that the physicality of α is somewhat neglected, and it is used strictly as a fitting parameter. Using α as a fitting parameter is commonly employed to achieve acceptable fits, such as in the method suggested by the NASGRO manual [12].

3.2.4 Least square fit

Finding the material parameters for the models according to the description above, requires a least square fit to $\mathrm{d}a/\mathrm{d}N$ test data. Threshold material data and critical stress intensity factor is taken from [13]. Taking the natural logarithm of the NASGRO equation (3.1) makes it possible to set up a least square fit for the material parameters C, n, p and q, according to equation (3.2).

$$\frac{\mathrm{d}a}{\mathrm{d}N} = C\left(\frac{1 - f\left(R, \frac{S_{\max}}{\sigma_0}\right)}{1-R}\Delta K\right)^n \frac{\left(1 - \frac{\Delta K_{\text{th}}(R,a))}{\Delta K}\right)^p}{\left(1 - \frac{K_{\max}}{K_c}\right)^q} \tag{3.1}$$

$$\ln\left(\frac{\mathrm{d}a}{\mathrm{d}N}\right) = \ln(C) + n\ln\left(\frac{1-f}{1-R}\Delta K\right) + p\ln\left(1 - \frac{\Delta K_{\text{th}}}{\Delta K}\right) - q\ln\left(1 - \frac{K_{\max}}{K_c}\right) \tag{3.2}$$

Here, the inputs to Newman's crack opening function R and $S_{\max}/\sigma_0$ varies with the data from each test, while α is kept constant. For the threshold level function, with material parameters from [13], $\alpha_{\text{th}} = 2.0$ and $(S_{\max}/\sigma_0)_{\text{th}} = 0.3$ is kept constant at default NASGRO values and R and a varies for each data point. The least square fit procedure is performed in MATLAB using the backslash operator.

3.2.5 Error measure

In order to decide the constraint factor value, a series of test calculations will be run. Selection of the best value for α will depend on when the calculation best resembles the test data. To determine when the calculation best resembles the test data, an error measure is needed. Many different error measures are found in the literature, but the most commonly used is the ratio of calculated number of cycles to the tested number of cycles. The disadvantage of this, as pointed out by Rudenfors [13], is that the shape of the crack growth curve is neglected. She proposed an error measure attempting to combine the shape accuracy and life accuracy of the prediction (equation (3.3)):

$$\gamma = \frac{A_{\text{test}} - A_{\text{calc}}}{A_{\text{test}}} \cdot \left| \frac{N_{\text{test}}}{N_{\text{calc}}} \right| \qquad A = \int_{a0}^{a1} N \mathrm{d}a \tag{3.3}$$

Here, $a0$ denotes start crack, $a1$ end crack and N number of cycles. A is thus the area to the left of the curve in an a versus N plot. There are some issues with this error measure. If the curves coincides, the first part will tend to zero while the second will tend to 1. Thus it is not clear if a minimum value or as close to unity as possible is desired. This could be a typographical error. Secondly, the area part may give zero error even if the curves do not coincide. The error measure used in this thesis will be the standard deviation of the life at each measure point in the test, equation (3.4):

$$\gamma = \sqrt{\frac{1}{N_{\text{datapoints}}}} \sqrt{\sum_{\text{i=1}}^{\text{Ndatapoints}} \left(1 - \frac{N_{\text{test}}(a_i)}{N_{\text{calc}}(a_i)}\right)^2} \tag{3.4}$$

Here $N_{\text{datapoints}}$ is the number of recorded data points from the test, $N_{\text{test}}(a_i)$ is the number of cycles at data point i with crack length a_i and $N_{\text{calc}}(a_i)$ is the number of cycles at crack length a_i. Only a simulation producing a growth curve which exactly matches the measured curve, will give zero in error with this error measure.

3.3 Analysis of missions

10 fan discs have been selected randomly to be analyzed, in order to get a representative selection of the entire fleet. In addition, one fan disc among those with most flying hours have been deliberately selected. For comparative analyzes, 18 bulks of 500 missions were created from the missions experienced by these 11 discs. For each disc the first 500 flight missions registered in the LTS database were selected as one bulk. Then, if there were more than 1000 LTS flight missions for that disc, another 500 flight LTS missions were put in a second bulk and so on. With this selection method, a mission bulk only gets missions from the same disc. Furthermore, only the time of those missions registered in the LTS database as flight missions was included. When crack growth occurs during a mission missing from the LTS database, or a ground mission, this will show as a vertical line in a crack length versus flight time plot.

The methodology for the analysis is similar to the one currently employed by GKN on the mix of virtual missions, but with the following differences.

- Different counting techniques are employed (unordered and ordered).
- Different material parameters, based on testing at more stress ratios, are used.
- In addition to the conventional Non-Interaction NASGRO equation, the Strip Yield model is used.
- Real missions are analyzed in sequence. Previously, a mix of generic missions were analyzed repeatedly until the critical crack size was reached, before averaging the results.
- Room temperature conditions are assumed throughout each mission, as this is the material test conditions.
- The crack case SC02 (figure 3.4) is used instead of SC17, due to compatibility with the Strip Yield model.

In addition to these methodological differences, another advantage with analyzing real missions is that motor ground usage can be included as well. This is currently not accounted for as only the time from clear to take-off to touchdown is reported. The effect of the excluded usage is investigated by evaluating the crack growth during the same time, for some individuals. The difference due to the simplification that the specimen is center-cracked, introduced by the crack case SC02, yields less than 0.01% change in SIF. This analysis was performed using the SC17 crack case and moving the crack from the location used by GKN to the center. The difference between the crack cases SC02 and SC17 (for equivalent input) is many orders of magnitudes larger. This is treated in appendix A.

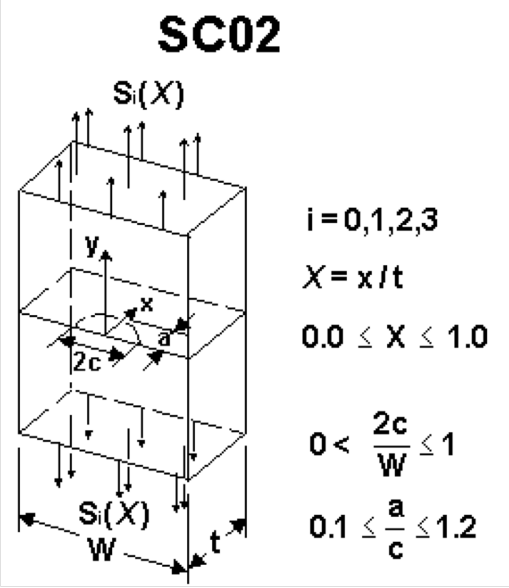

Figure 3.4: *Crack case SC02 [12]*

3.4 Effect of cycle counting technique

The method used when analyzing missions implies that each mission comes in order with respect to each other. The cycle counting will thus be performed separately for each individual mission, so there are two main differences that may occur for different counting techniques:

1. The severity and number of cycles counted

2. The order within each mission the cycles occur

To evaluate the effect of choosing different counting techniques, some missions will be analyzed to investigate how much the results differ for various counting techniques. The rainflow count routine is chosen since it is the most commonly used [28], and it is also the method of choice at GKN. This choice eliminates variations due to item number 1 above, leaving only the order left to influence the results. Choosing more simple counting methods such as level crossing would neglect cycles, thus it may be nonconservative. By modifying the rainflow count routine, according to suggestion by [29], to locate each cycle in the order that it's tensile peak occur, a rainflow count routine that is affected by the order in which the loads occur is achieved. This methodology is doubtful since it is not only the tensile overload that causes history effect, but also lower loads may contribute to differences in history effects due to a reduction in retardation effects. The purpose of having these two methods is not to find which is the more accurate, but to determine if altering the orders of cycles within each mission has a significant effect on the total crack growth. Should this turn out to greatly affect propagation speeds, it indicates that more research is needed to translate mission load history into cycles. To decide the influence of the counting technique, only the Strip Yield model will be used.

3.5 Treatment of missing missions

A challenge with using the data supplied to the LTS system, is that not all missions are registered for various reasons. An older system which only registers full and partial cycles, based on a level crossing counting procedure [1], includes a higher fraction of the missions. The contribution to crack growth from missions missing from this database is assumed to be negligible. The crack growth for real missions (Δa^{NH}) can be described as function of initial crack length (a_0), number of partial NH cycles ($\mathrm{NH_p}$) and probability of being conservative in the approximation (p). Furthermore, the crack growth for artificial missions (Δa^{NL}) is given as a function of initial crack length and number of artificial NL cycles ($\mathrm{NL_p}$). This is calculated for a spectrum consisting of 1 full NL cycle and $\mathrm{NL_p} - 1$ partial NL cycles. The NL cycles are defined by taking the average value of the lower pressure shaft rotational speed for a large number of datapoints with the high pressure shaft rotation speed equal to the level crossing values. The exception is that zero speed is given as lowest point in the full cycle, as it is known that this state will occur at the start and end of each mission.

$$\Delta a^{\mathrm{NH}}(a_0, \mathrm{NH_p}, p) \tag{3.5}$$

$$\Delta a^{\mathrm{NL}}(a_0, \mathrm{NL_p}) \tag{3.6}$$

A typical mission has less than 10 μm crack growth in the corner cracked disc. As the corner crack case in the disc is the most critical with the highest crack growth rate, it is used to verify the herein described method, using material data for the fan blades due to availability. This ensures that the assumption that the growth rate during one mission depend only on the loading and the initial crack length. The purpose of this treatment is to replace the loading from a mission not registered in LTS with an equivalent load history based on the number of partial NH cycles registered. Therefore, the loading will be fully described by $\mathrm{NH_p}$ or $\mathrm{NL_p}$. Based on these arguments, the above equations can be rewritten, by introducing the geometry independent $\Delta a_*^{\mathrm{NH}}(\mathrm{NH_p}, p)$ and $\Delta a_*^{\mathrm{NL}}(\mathrm{NL_p}, p)$, and the loading independent $g(a)$, as

$$\Delta a^{\mathrm{NH}}(a_0, \mathrm{NH_p}, p) = g(a)\Delta a_*^{\mathrm{NH}}(\mathrm{NH_p}, p) \tag{3.7}$$

$$\Delta a^{\mathrm{NL}}(a_0, \mathrm{NL_p}) = g(a)\Delta a_*^{\mathrm{NL}}(\mathrm{NL_p}) \tag{3.8}$$

Maintaining the assumption that the change of $g(a)$ is negligible during one mission, it can be assumed that $\Delta a^{\mathrm{NL}}(a_0, \mathrm{NL_p}) = g(a_0)\,(A_0 + A_1\mathrm{NL_p})$. This should be true since the equivalent spectrum has one initial large cycle (full NL cycle) followed by a number of smaller partial NL cycles. The first cycle will give more crack growth than the following cycles, thus the constant term is needed. After this, since the crack length is assumed constant and the loading is CA, $\mathrm{d}a/\mathrm{d}N$ is constant. Thus the change in crack length after the initial large cycle is proportional to the number of NL cycles. From this, the equations can be combined by setting $\Delta a^{\mathrm{NL}} = \Delta a^{\mathrm{NH}}$:

$$g(a_0)\,(A_0 + A_1\mathrm{NL_p}) = g(a_0)\Delta a_*^{\mathrm{NH}}(\mathrm{NH_p}, p) \tag{3.9}$$

$$\mathrm{NL_p} = \frac{1}{A_1}\left(\Delta a_*^{\mathrm{NH}}(\mathrm{NH_p}, p) - A_0\right) \tag{3.10}$$

In order to find the function $\Delta a^{\mathrm{NH}}(a_0, \mathrm{NH_p}, p)$, a large number of individual missions will be analyzed with different $\mathrm{NH_p}$, for a specific a_0. Two linear approximations will then be developed, for the crack growth mean and standard deviation as a function of number of NH cycles. The function $g(a_0)$ becomes arbitrary as long as the constants A_0 and A_1 is found for the same initial start crack.

3.6 Sensitivity analysis

In order to evaluate the accuracy of the models proposed, without sufficient available test data, an analysis of factors that influence the solution will be performed. The purpose of this analysis is to determine which parameter of the method that has the most significant effect on the end result. This will guide future work on what part of the method that should be improved. To see the differences between the currently used Non-Interaction NASGRO equation and the Strip Yield interaction model, results from these two models will be compared. The material calibration is performed on the same CA testing for both models, so the differences should be due to the spectrum effects. Large differences will indicate the need for the more advanced Strip Yield model, since this would show that the Non-Interaction model is unable to give fair predictions for spectrum loading.

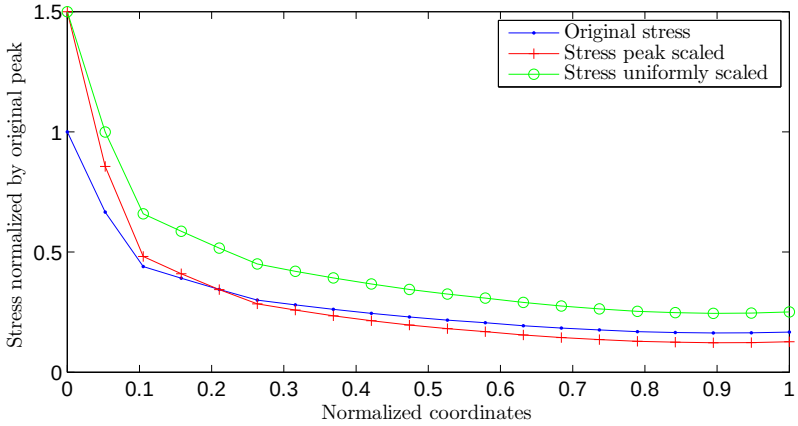

Figure 3.5: *Demonstration of stress field scaling*

To evaluate the importance of the accuracy of the stress field, the influence of altering the stress field in two ways is evaluated. Firstly, the entire stress field is scaled uniformly with a scale factor of 1.01 and 1.10. Secondly, the peak value is increased by a scale factor of 1.01 and 1.10, while maintaining constant average stress in the section. The latter scaling is achieved by raising the normalized stress $s(x)$ to a power k. An iterative solver in MATLAB searches for a value of k so that the one dimensional stress field required for the crack case SC02 maintains a constant mean value when multiplied with the specified scale factor. Figure 3.5 demonstrates how the stress field is altered, both through uniform scaling and peak scaling.

Newman [30] is one of many suggesting that the α parameter in the Strip Yield model should be calibrated using single peak overload tests. This has not been possible within this thesis as no such tests have been performed at GKN, and additional physical testing is as previously mentioned out of scope. To evaluate how important it is to perform these tests to obtain a better value for α, a series of simulations of real missions with different values of α in the Strip Yield model will be performed. These will serve as basis for recommendation for future experimental needs.

4 Results

4.1 Material data calibration

Rudenfors [13] was unable to produce a distinct minimum when varying α and $S_{\max}/\sigma_0$ to generate a set of material data. Using the proposed error measure in combination with using the actual value of $S_{\max}/\sigma_0$ during tests, a value of α producing a distinct minimum of mean error was found, see figure 4.1a. Analyzing the error for each test individually, it is clear that the mean by itself does not tell the full story. Setting the objective to minimize the the maximum error, instead of the mean, results in a different value of α, see figure 4.1b. From this plot it can be seen that the error varies significantly between the individual tests, compared to the variation of the mean value with α. Thus it is clear that the effect of calibrating material data with different values of α is much smaller than the inaccuracy of the NASGRO equation model and the uncertainties in the tests. The chosen material data are based $\alpha = 1.7$ producing the the minimum value of the mean error ($\gamma = 0.1551$).

Table 4.1: Calibrated material data for NI- and SY-model

Parameter	Value (NI)	Value (SY)	Unit
α	1.7	1.6	-
C	$1.5682\text{e}-12$	1.7618×10^{-12}	$\text{MPa}\sqrt{\text{mm}}$
n	2.9883	2.9489	-
p	0.3150	0.3737	-
q	0.0195	0.1055	-

The Strip Yield model material parameters were calibrated using the previously described method, resulting in figure 4.2. The magnitude of the mean error was comparable to the Non-Interaction model. It should be noted that choosing material data (C, n, p and q) equal to the Non-Interaction model yields a higher mean error, thus indicating that the method proposed in [12] may not give the best material data set. On the other hand, the optimum value of α for the Non-Interaction model may be hard to determine due to the large test data scatter. Furthermore, it can be seen that changing the constraint factor for the Strip Yield model (α_{SY}) does not have as large effect on the results as altering material data (i.e. α_{mp}). This observation is supported by [30], suggesting to use single-spike overloads to determine α for calibrating the Strip Yield model. The fitted material data for both the Non-Interaction model and the Strip Yield model is given in table 4.1. The remaining material parameters used can be found in [13].

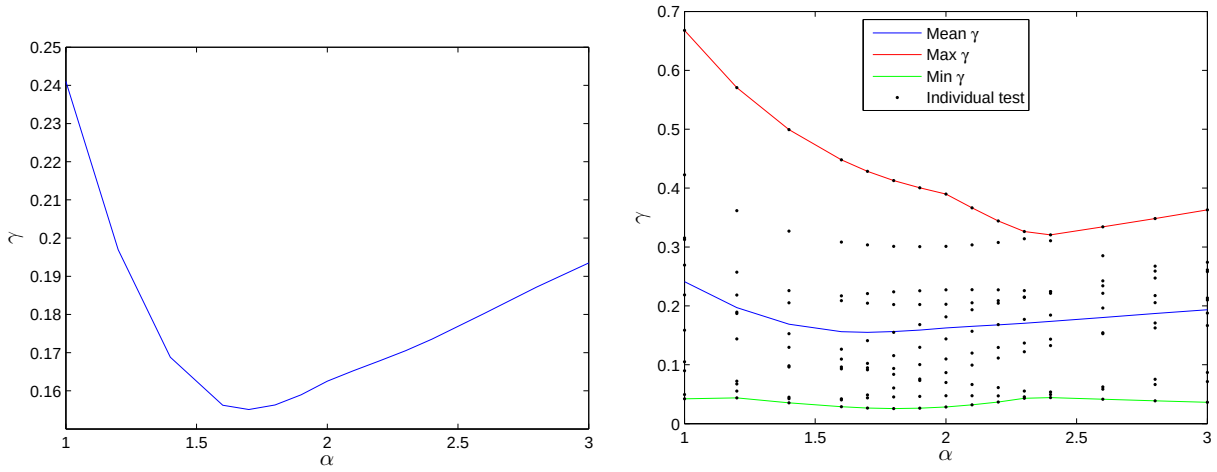

(a) *Mean error*

(b) *Errors of individual experiments*

Figure 4.1: *Error measure(γ) versus constraint factor (α) for CA model material data calibration*

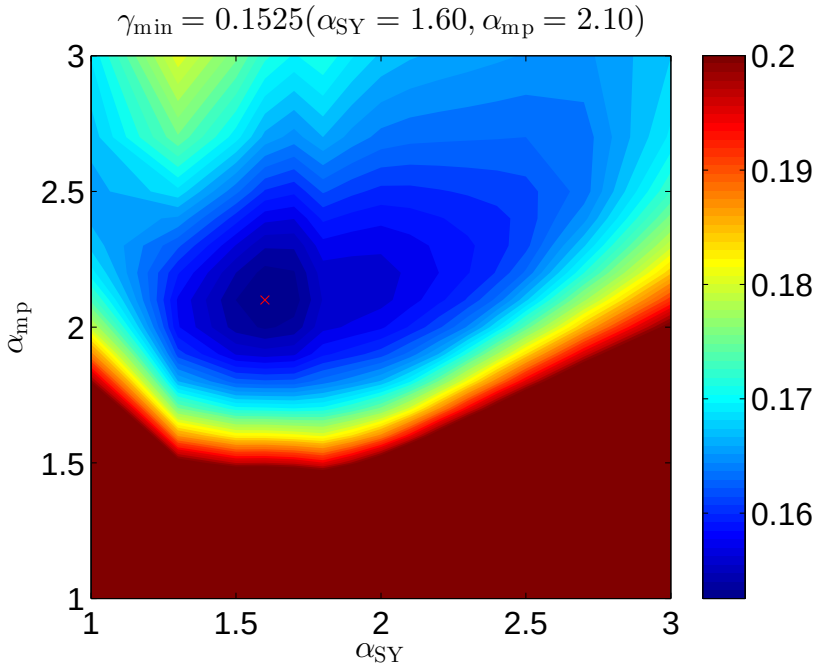

Figure 4.2: *Calibration of Strip Yield material parameters and tensile yield constraint factor (α_{mp} denotes the constraint factor used to determine material parameters and α_{SY} denotes the constraint factor used in the Strip Yield model)*

4.2 Comparison with spectrum crack propagation

The shape of the spectrum crack propagation experiment crack growth curve depends on the finite element simulation of the potential drop. The potential drop at the 11 simulated crack lengths is used to create least square fit 2nd degree polynomial to translate potential drop into crack length. The largest difference between a simulated point and the fit was 1.7%. The error introduced by placing the probe at the edge of the specified tolerance area, compared to the center gave maximum 0.4% difference. Doubling the notch size gave a difference of less than 0.02%. As long as the test is performed according to specifications, it is from here on assumed that these differences can be neglected.

The test conditions were analyzed as described in the method section, both using the Strip Yield model and the Non-Interaction NASGRO equation. In the latter the load parameter S_{max}/σ_0 was set at both the mean

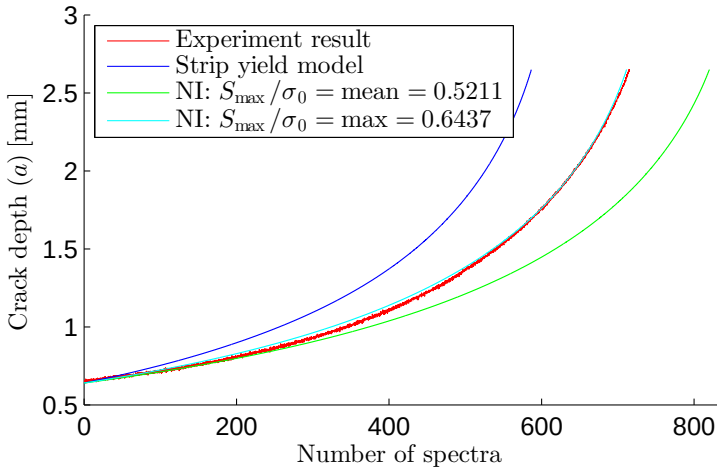

Figure 4.3: *Comparison of proposed models to the RM12 spectrum crack growth experiment*

value for the peaks of the spectrum and the maximum value. As can be seen from the plots in figure 4.3, the Non-Interaction model with maximum value for the load parameter correlates very well with the experiment. It is also clear that this parameter is very influential on the Non-Interaction model. The Strip Yield model also produces reasonable results, but quite conservative. The Non-Interaction model with mean value for the load parameter, is on the other hand equally non-conservative as the Strip Yield model is conservative. The results in this section should be analyzed with caution though, as it is only based on one experiment at one load level. Further analysis of more missions will give further indications on the applicability of the simple Non-Interaction model, compared to the Strip Yield model.

4.3 Effect of counting technique

In order to evaluate the effect of counting technique, the 18 bulks of missions were simulated up to 150 flight hours, from a start crack of 0.63mm. All missions reached a bigger crack when employing the rainflow count method maintaining the order of peaks. The largest difference was 2.07% more crack growth, while the average difference was 0.99%. As discussed in the method section, it is not possible to define an ordered rainflow cycle counting which gives a correct representation, since there will be small cycles between the peak and valley of a larger cycle. The results indicates that for the given spectra the effect of the ordering within each mission is small when compared to other uncertainties. An example of these uncertainties can be seen in the comparison between predicted and measured result for the spectrum crack propagation test in figure 4.3.

4.4 Treatment of missing missions

As described in the method section, a methodology to analyze missions missing from the LTS database was developed, based on information from the old level-crossing counting system. Analyzing all available missions from a start crack depth of 1 mm, the mean crack growth from each mission as a function of number of partial NH-cycles could be calculated. Furthermore, the standard deviation for each number of partial NH cycles was calculated as well. Using this information, figure 4.4 could be created. Here, linear approximations of the mean and standard deviation of crack depth change as a function of number of partial NH cycles ($\mathrm{NH_p} > 0$) was plotted as well. These linear approximations are then used for making a function translating the number of NH cycles into an equivalent spectrum of NL cycles.

In order to ensure that the methodology is independent of the stress intensity factor solution, in particular the crack length, a second fit based on simulation from a different start crack was made. Since the purpose of the methodology is to translate loads, it should be independent on crack length according to the arguments

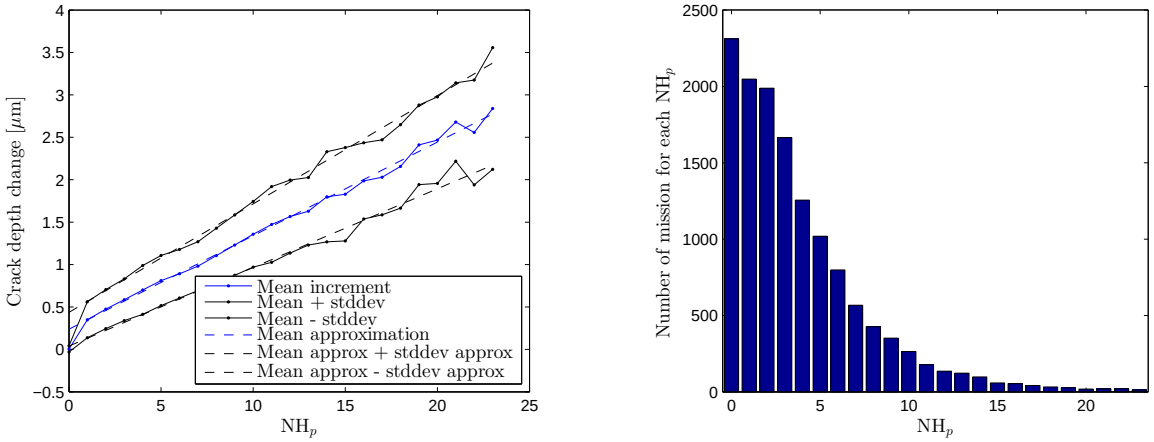

(a) *Mean and standard deviation linear fits of* $\Delta a(NH_p, a_0 = 1\text{ mm}, p)$

(b) *Statistical basis used in figure* (a)

Figure 4.4: *Average crack growth per mission as a function of registered partial NH-cycles based on analysis of all available missions at a semi circular start crack of depth* 1 mm

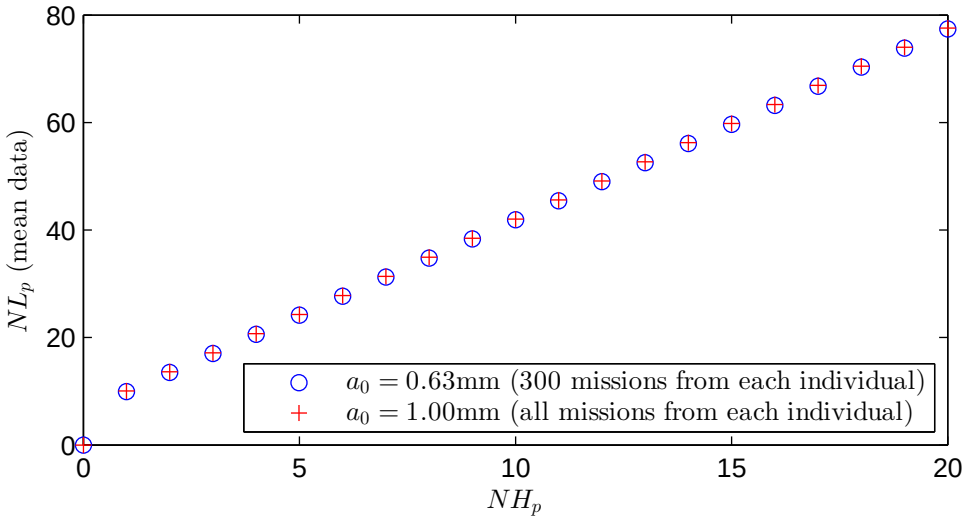

Figure 4.5: *Illustration of start crack independence for the analysis used to generate a function describing equivalent number of partial NL-cycles as a function of partial NH-cycles*

given in the method section of this thesis. In figure 4.5, a plot of both functions for different values of NH_p is given, showing that there is virtually no difference between the results from start crack depth 0.63 mm and 1.00 mm, both using the average crack depth change. The current implementation used for analysis of real missions rounds the number of partial NL cycles upwards, in order to be conservative. The rounding error will never exceed 10% with this methodology for missions with 1 partial NH cycle, since the equivalent number of NL cycles is 10 and the full cycle is significantly more influential than a partial cycle. To improve the accuracy, at the expense of conservatism, it would be possible to round downwards while keeping track of the lost fraction of cycles and add one cycle once the sum of fractions give a cycle. This has not been implemented for this thesis.

Analyzing all 18 mission bulks using the CA model with the load parameter $S_{\max}/\sigma_0 = 0.3$, the difference between using using the logged data from the LTS database and this method based on registered partial NH cycles, was on average 7.0%. The maximum difference was 22.6% and the minimum was -2.7%. So in general the method described above gives a conservative prediction when the mean data for crack growth per partial NH-cycle is used. The distribution of difference in crack growth is given in figure 4.6.

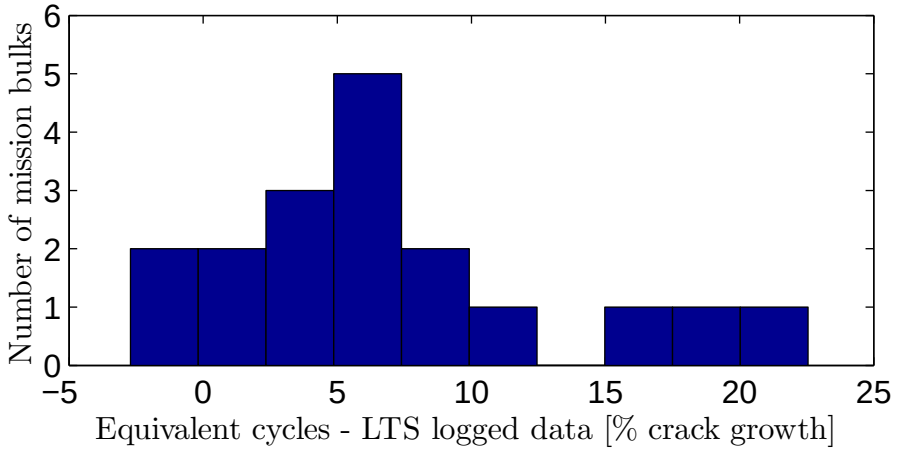

Figure 4.6: *Comparison between crack growth based on equivalent cycles (generated using the herein described method for missing missions) and logged data, using the NI-model with* $S_{\max}/\sigma_0 = 0.3$

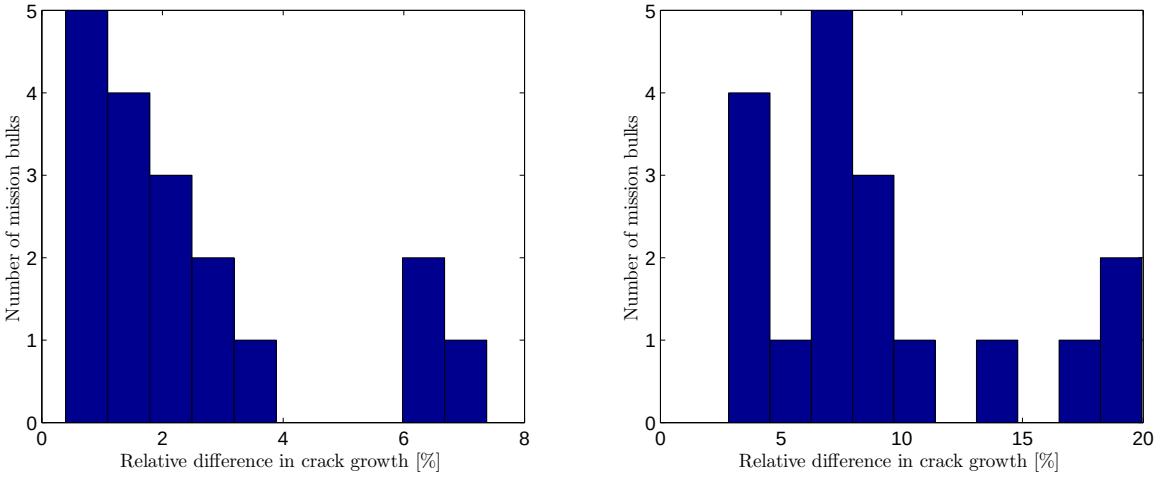

(a) *Effect of adding only ground missions* (b) *Effect of adding ground and missing missions*

Figure 4.7: *Importance of ground and missing missions on crack growth using the NI-model*

4.5 Importance of ground and missing missions

In order to evaluate the importance of incorporating ground missions and missing missions in the analysis, the 18 bulks of flight missions were analyzed individually using the NI-model. During the time interval of those missions, for each fan disc, the old life tracking database was searched for missions not included in the new LTS database. These missions were then added based on the number of partial NH cycles, using the methodology as described earlier. All mission bulks were analyzed starting from a semi circular crack with depth of 0.63 mm. The reference solution is an analysis of only flown missions from the LTS database, and figure 4.7 show the distribution of relative difference in crack growth when adding only ground missions and when adding both ground and missing missions. The average additional crack growth when taken ground missions into account was 2.47%, while adding both ground and the missing missions resulted in an average increase of 9.08% crack growth.

4.6 Variation between discs

4.6.1 Strip Yield model

When calculating the life based on a set of generic missions, the goal is to set the load levels so they are representative of the individual subjected to the toughest use. The advantage of individually tracking the use of each disc is that the load levels used in calculations can be aimed at representing the levels experienced by the disc. From this argument, it becomes natural to evaluate the potential savings associated with following up each disc individually by comparing the life of all discs to the individual with shortest life. In figure 4.8 the

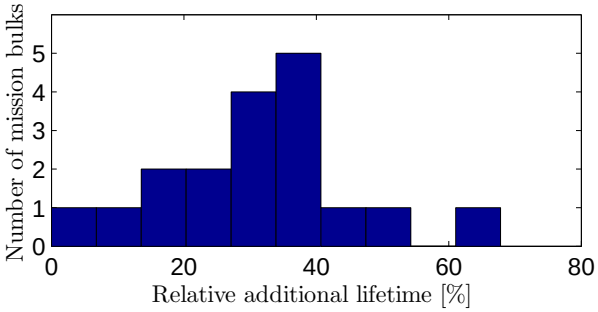

Figure 4.8: *Additional lifetime compared to the most severe bulk, using the Strip Yield model*

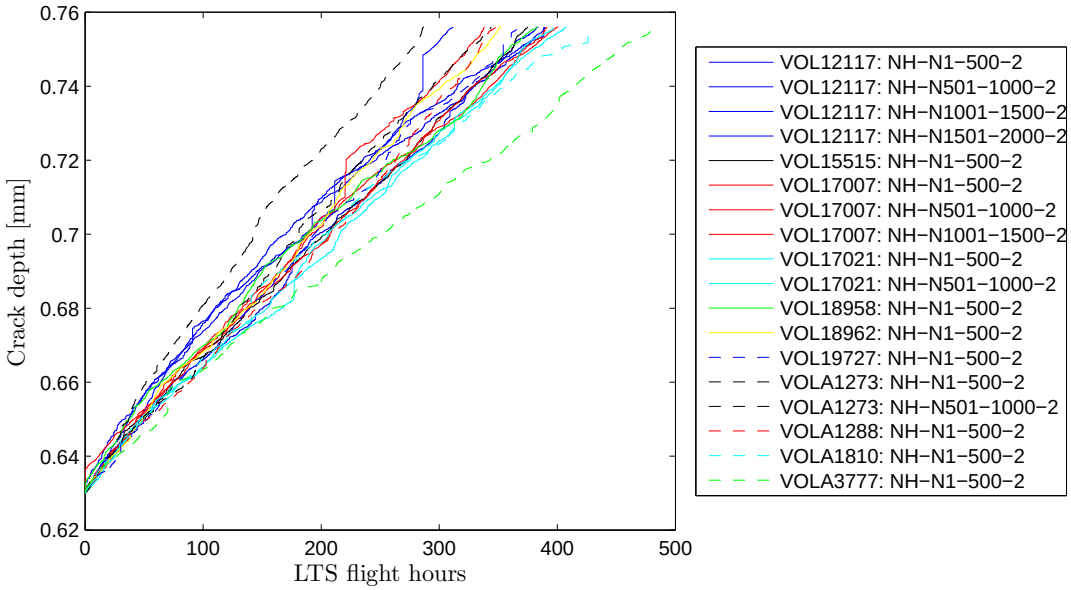

Figure 4.9: *Crack growth for each mission bulk using the Strip Yield model. The number VOLnnnnn denotes which motor individual the bulk is for, and N1-N500 denotes flight LTS mission 1 to 500 for that motor*

relative lifetime of all analyzed individuals compared to the shortest life is given. The time is taken at the point of reaching the shortest crack size achieved amongst all bulks of missions. To further illustrate how the cracks develop during a mission, a plot of crack length versus flight hours is given in figure 4.9. The average additional life compared to the shortest of the 18 mission bulks analyzed was 31.1% and the maximum was 67.8%.

4.6.2 Non-Interaction model

When performing the same analysis as above for the Non-Interaction model, slightly smaller differences are found. The calculated average additional life was 25.5% and the maximum additional life was 60.3%. As mentioned above, it is natural to assume that the mix of generic mission currently used (A3B3-mix) should represent the loading on the most severely loaded disc. In figure 4.10 the average crack growth from the A3B3 mix is plotted, together with crack growth curves for the batches of missions. The average mix crack growth has been calculated using the average of time spent to reach distinct crack sizes for all missions within the mix, weighted by their assumed frequency of occurrence. The plot of the LTS missions shows the growth for the

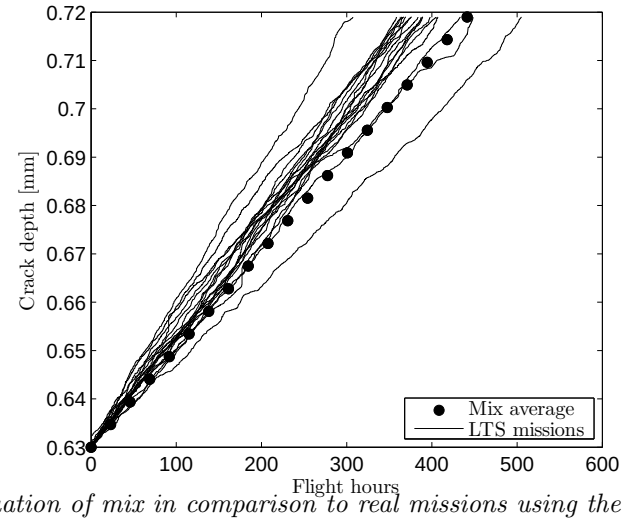

Figure 4.10: *Evaluation of mix in comparison to real missions using the Non-Interaction model*

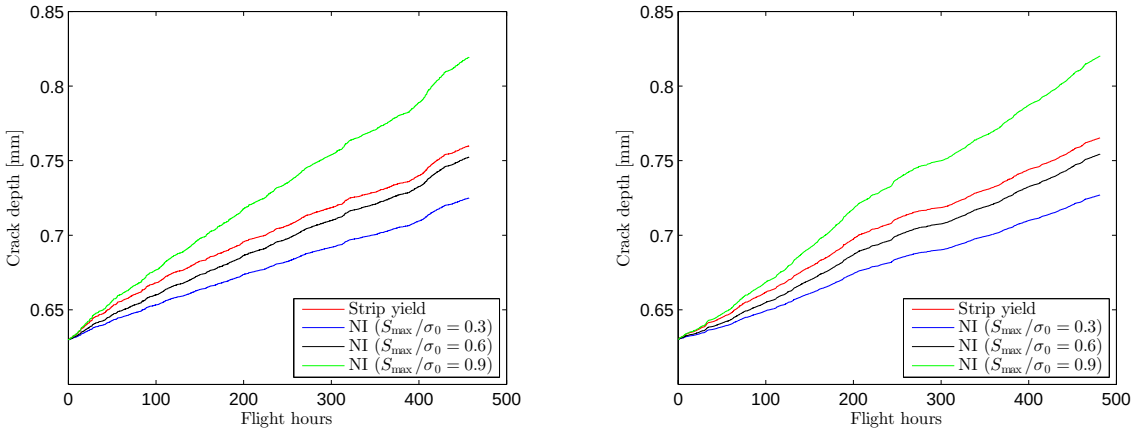

(a) *VOL12117 - Flight mission 1-500* (b) *VOL19727 - Flight mission 1-500*

Figure 4.11: *Differences in crack growth between the Strip Yield model and Non-Interaction model for two selected bulks of missions*

mission bulks taking flight and ground missions registered in the LTS database into account. All data has been calculated using the NI-model with $S_{\max}/\sigma_0 = 0.3$ and crack case SC02. From the plot it becomes apparent that the currently used mix data is not conservative for the majority of the individuals. On the contrary it seems to be representative of the least loaded individuals.

4.7 Sensitivity analysis

4.7.1 Differences between crack propagation models

During the material data calibration, the Strip Yield model and the Non-Interaction model achieved similar errors for CA test data. Spectrum testing revealed quite significant differences, and it was clear that the load parameter had sufficient effect on the result to fit the Non-Interaction model to the test data. To further evaluate the differences, the results from simulations of two real missions are compared in figure 4.11. It should be noted that for the analyzed fan blade the maximum load parameter, taking the maximum stress location at maximum revolution speed, is $S_{\max}/\sigma_0 \approx 0.78$. The growth curve from these two missions clearly show that the load parameter has a significant effect on the result. The Strip Yield model is between the curve for $S_{\max}/\sigma_0 = 0.6$ and $S_{\max}/\sigma_0 = 0.9$, but much closer to the 0.6 curve. Analyzing the resulting end crack after all LTS flight missions used (figure 4.12), it can be seen that the trend from the above examples is maintained for all bulks of missions. The majority of the difference in mission bulks for $S_{\max}/\sigma_0 = 0.6$ are within a scatter

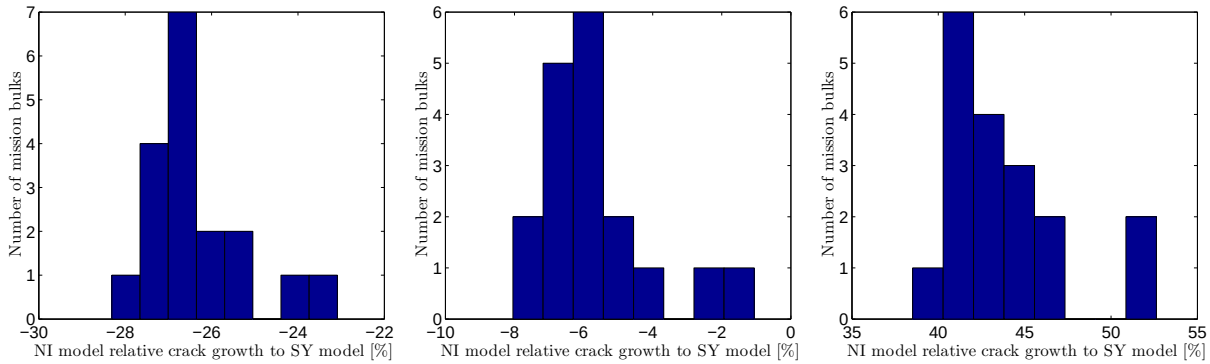

(a) $S_{\max}/\sigma_0 = 0.3$ (b) $S_{\max}/\sigma_0 = 0.6$ (c) $S_{\max}/\sigma_0 = 0.9$

Figure 4.12: *Distribution of differences in crack growth of the Strip Yield model and Non-Interaction model*

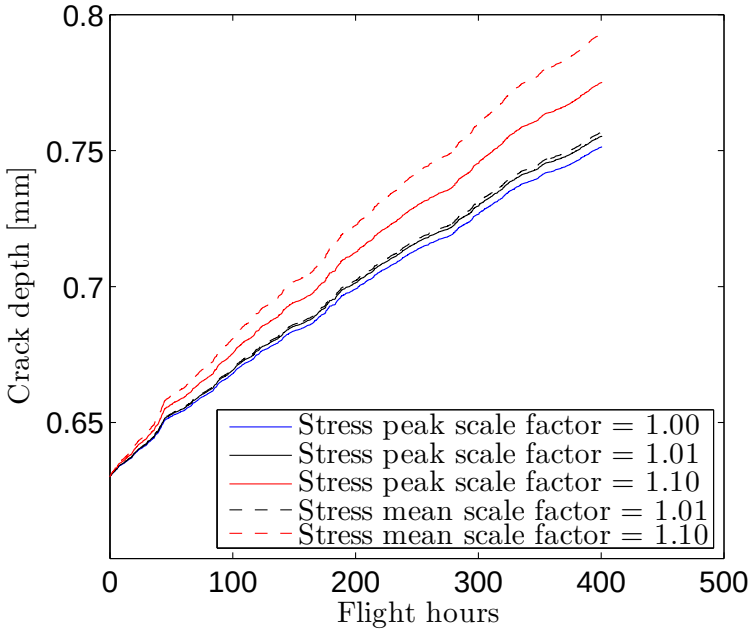

Figure 4.13: *Crack growth for one bulk of 500 missions using the Strip Yield model with different stress field scaling*

band of ±2%. This indicates that the Non-Interaction model can be calibrated to fit the Strip Yield model by altering the load parameter. Due to the large effect of the load parameter for the Non-Interaction model, it is clear that material data needs to be found experimentally for correct load levels.

4.7.2 Effect of stress field inaccuracies

By both altering the peak stress while maintaining constant mean stress, and altering the whole stress uniformly, the crack growth sensitivity to the stress field can be evaluated. Figure 4.13 is an example of how this affect a bulk of missions. As easily seen from the fracture mechanics equations, altering the stress field uniformly linearly scales the SIF. From the NASGRO equation it can be seen that increase in crack growth rate then should be the scale factor to the power of $n \approx 3$. Thus scaling the stress field uniformly, has a big impact on the crack growth rates as seen in 4.13. The average increase in crack growth was 4.5% for a 1% uniform raise in stress level, and 35% for a 10% raise. This is slightly higher than predicted by the simple analysis of the NASGRO equation, raising the scale factor to the power of n. The simple analysis is only valid for the Paris region of the crack growth, and does not take into account the effect of a larger yield zone or smaller cycles going above the threshold limit. The effect of increasing the peak stress while maintaining a constant mean stress in the section has a quite large effect on the growth rates as well. This change in the stress field is also a more likely result of insufficient accuracy in FE-simulations, than an error in the average stress. A 1% increase in the peak stress resulted in an average increase in crack growth of 3.3%. Increasing the peak stress by 10% yielded an average increase of 20%. As expected the effect is smaller than increasing the entire stress field, but perhaps more important as [31] approximates the error in [8] to be up to 10% in the stress field.

4.7.3 Importance of the Strip Yield constraint factor

Results from analyzing all the mission bulks with different values of α in the Strip Yield model gives more crack growth with larger values of the constraint factor. This is expected as higher values implies less tensile yielding and lower closure levels. The average difference between crack growth for $\alpha = 1.0$ and $\alpha = 3.0$ was 28%, and the maximum difference was 39%. An example of the different crack growth curves produced when varying α is given in figure 4.14. From the results it is clear that α have a significant influence on the result, similar to altering the stress level with 10% as seen in the previous section.

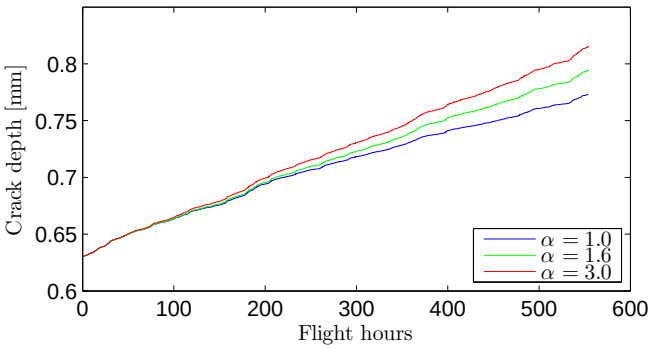

Figure 4.14: *Influence on result of varying the Strip Yield constraint factor* α

5 Discussion

5.1 Crack propagation model

Based on the literature research presented in section 3.1, Newman's constant constraint loss Strip Yield method was chosen, due to its possibility to model both interaction effects and accounting for varying load levels. During the work with the thesis it has become evident that the implementation of the Strip Yield model in NASGRO is not clearly defined for all crack configurations. In appendix A there are unexplained examples of differences between seemingly equal cases. The description given in the manual [12] mostly treats through cracks and the applicability to more complicated crack cases may be debated. Based on the discussion in section 3.1, it is clear that the Strip Yield model has advantages over the other interaction models, making it the most promising candidate to simulate real spectra. An issue with many interaction models is that they are able to simulate simple VA-loading, such as single spike overloads, but they lack the physicality required to analyze more complex loading spectra. The Non-Interaction NASGRO-equation has proven to give consistent results in relation to the Strip Yield model. This indicates that most missions give similar loading conditions, and that the interaction effects may be smaller than expected. This means that the Non-Interaction NASGRO-equation could be calibrated by the load level to give correct results for the spectrum loading conditions experienced during real missions. Such calibration would require spectrum testing of component like specimens with similar stress gradients. If such testing is required, the Strip Yield model could on the other hand be expected to produce better results with fewer tests, due to its better physical background. The current uncertainties in the implementation in NASGRO regarding the Strip Yield model do pose some risks which should be sorted out before using the Strip Yield model in a critical analysis. Questions to the NASGRO development team has been sent addressing these issues, but at the time of writing no reply has been received.

5.2 Analysis of real missions

An average difference in life of 31.1% and 25.5% compared to the most severe of 18 bulks of 500 LTS missions was found for the Strip Yield and Non-Interaction model respectively. In combination with maximum differences of 67.8% and 60.3%, this indicates that there is a large potential to save in number of inspections if each individual is followed up. Since the analysis of the mix showed a longer than average life than the same analysis for real missions, it does not appear to be possible to save many inspections. The higher accuracy in the method gained from using measured speed may, however, allow the use of a lower safety margin. This can in its turn allow for longer inspection intervals for some individuals. More importantly, implementing individual follow up will decrease the risk of failure which is critical in the investigated application.

5.3 Recommendations for implementation in LTS

One aspect of using an interaction model, which was considered initially, was the importance of a counting technique keeping track of the order of cycles. Based on this the ordered counting method as proposed by Newman was implemented. It did not affect the results to a large extent compared to other uncertainties, as previously noted. Thus for the implementation in LTS this is not considered a high priority. A standard rainflow counting technique can be used for each individual mission, and then these counted missions can be put together for a complete analysis. Thus the order between each mission is maintained. This methodology is possible since all missions are assumed to start and end at zero stress level, and there are only positive principal stresses.

The effect of ground missions was about 2.5 times more influential than the counting technique differences, and is much easier to implement. This is also important as it is guaranteed nonconservative to neglect the ground missions. Using the proposed method to handle missions not in the LTS database, it showed together with ground missions an increase in crack growth of 9.1% compared to the flight missions in the LTS database. Thus this effect is very important to implement if the crack propagation failure mode should be used in LTS. The proposed method showed good promise in terms of independence of the start crack. It has potential to be more accurate than flight time only, as it can incorporate both ground missions and flown mission in addition to analyze loading based on the actual use. The comparison to using real mission data showed that this method is conservative by an average 7% more crack growth. The extreme values were 22.6% and -2.7%. If the goal is

to be more accurate, the method could probably benefit from implementing the improvements suggested in section 4.4. A final issue with the method used to calibrate the translation of the level crossing counting cycles to an equivalent spectrum, is the fact that the analysis is based on missions registered in the LTS database. These may not be statistically representative of the missions missing from the same database.

It is clear that the accuracy of the finite element stress analysis can greatly influence the results. As noted previously, a 10% increase in peak stress while maintaining constant mean stress gave 20% higher crack growth. This difference is of equal magnitude to the difference between the Strip Yield and Non-Interaction model, with reasonable values of $S_{\max}/\sigma_0$.

Implementing crack growth modeling in LTS using the Strip Yield model is not recommended by the author at the current knowledge level regarding its implementation in NASGRO. The discrepancies in NASGRO's behavior compared to the manual and between crack cases when using the Strip Yield model pose a significant risk to the reliability of the simulations. Since it appears to be possible to adjust the Non-Interaction NASGRO equation to the spectrum cases by altering the load parameter, this is considered a better option. The advantage of using a well documented and predictable Strip Yield model implementation is that the requirements on testing can be reduced. The reason is that the Strip Yield model should, in theory, better model variations in load levels and spectrum type due to its theoretically more physical foundation.

To improve the understanding of the load parameter, the author would recommend to test both spectrum and constant amplitude loading on specimens with stress gradients similar to those found in the real application. These tests should be designed to give an understanding of how the load parameter should be changed dependent on the analyzed loading situation. For future use of the Strip Yield model, single spike overload tests are required to determine a value of α. For the Strip Yield model it would be sufficient to verify against more spectrum tests as this model doesn't require user input of a load parameter.

6 Conclusion

Based on the results presented in this thesis, the implementation of the crack propagation failure mode for the fan stages is highly recommended. Based on 11 different fan discs in stage 2, 18 bulks of 500 LTS missions were created. The average differences in life to the most severe bulk was between 25.5% and 31.1%, depending on crack propagation method used. This implies that given equal safety factor for the most severely loaded individual, the inspection interval can be increased by over 25% yielding an 20% inspection cost saving. An analysis with the current methodology, using a predefined mix, revealed that this method is nonconservative. Thus the current safety margin for the toughest loaded individual should be considered increased to avoid failures. In either case, analysis of the actual loading on each individual will be a significant improvement over the currently used method.

The recommendations for implementation of this methodology into LTS are summarized as follows

- Until the implementation and description of the Strip Yield method in NASGRO is improved, the use of the Non-Interaction model should be continued.
- Maintaining order of cycles within each mission has very little effect, so this can be neglected even when using the Strip Yield model.
- Fatigue crack propagation testing at both CA and spectrum loading of specimens with stress gradients similar to those of the actual components should be carried out, in order to improve the understanding of the load parameter. The NASGRO equation parameters should be calibrated using the actual value of the load parameter from the currently existing CA tests. The same SIF solution used in the NASGRO software needs to be employed during test result reporting.
- If the Strip Yield model should be used in the future, experiments with single spike overload(s), followed by CA loading, should be carried out in order to obtain reasonable values for the plastic constraint factor α.
- Ground missions should be included in the analysis as this is easily implemented and increased the average crack growth rate with about 2.5%
- Missions not in the LTS database should be analyzed. This can be accomplished by using the equivalent load methodology proposed in this thesis, but its accuracy should be further verified before implementation.
- The currently used stress solution [8] should be analyzed further in order to more accurately estimate the magnitude of the stress error, as the stress gradient can significantly alter the crack propagation rate.

References

[1] M. Andersson. "Life tracking system (LTS) for RM12". *International Symposium; 20th, Air breathing engines; ISABE 2011*. American Institute of Aeronautics and Astronautics Inc, Reston, VA, USA. 2011, pp. 1957–1965.

[2] W. Elber. "The significance of fatigue crack closure". *Damage tolerance in aircraft structures ASTM STP 468 Philadelphia, USA: American Soceciety for Testing and Materials* (1971), pp. 230–242.

[3] L. Samuelsson. *Investigation of sequence effects on fatigue life. Material dependence*. GKN Internal Report: 2005VAC003023, Trollhättan, Sweden. 2005.

[4] VAC. *RM12 Allmän kurs*. GKN Internal Documentation, Trollhättan, Sweden. 2002.

[5] J. Städje (2008). URL: `http://techworld.idg.se/2.2524/1.174315/reaktionsmotor-12---bade-vacker-och-stark` (visited on 05/23/2014).

[6] J. Ohlsson. *Beskrivning av inspektionsmatris för fläktskiva 2 och fläktskiva 3 för RM12 inom DTU verksamheten*. GKN Internal Report: VOLS: 10042639, Trollhättan, Sweden. 2007.

[7] J. Olsson. *Sprickpropageringsanalys af fläktsteg 2 (96011770) i RM12*. GKN Internal Report: VOLS: 10182060, Trollhättan, Sweden. 2013.

[8] J. Olsson. *Spänningsanalys av skovelinfästning mellan fläktskiva 2 (P9601770) och fläktskovel 2 (P9606354) RM12*. GKN Internal Report: VOLS: 10107223, Trollhättan, Sweden. 2013.

[9] P. Nilsson. *POD-analys ET Fläktskiva 1, 2 och 3 RM12*. GKN Internal Report: VOLS: 10191515, Trollhättan, Sweden. 2014.

[10] P. Nilsson. *POD-analys ET Fläktskovel 1, 2 och 3 RM12*. GKN Internal Report: VOLS: 10173726, Trollhättan, Sweden. 2012.

[11] J. Olsson. *Referensdokument för sprickpropageringsanalyser i fläkt RM12*. GKN Internal Report: VOLS: 10179643, Trollhättan, Sweden. 2013.

[12] NASGRO. *Fracture Mechanics and Fatigue Crack Growth Analysis Software, Reference Manual*. Version 7.0 Final. 2012.

[13] M. Rudenfors. *Crack propagation rate material data handling using NASGRO*. GKN Internal Report: VOLS 10033403, Trollhättan, Sweden. 2006.

[14] T. Hansson and T. Månsson. *Slutrapport Methodutveckling Sprickpropagering RU2004*. GKN Internal Report: 9650-1482, Trollhättan, Sweden. 2004.

[15] M. Rudenfors. *Sequence effects in Ti6-4 and In718 for RM12 load spectra*. GKN Internal Report: VOLS 10032362, Trollhättan, Sweden. 2006.

[16] N. E. Dowling. *Mechanical Behaviour of Materials. Engineering Methods for Deformation, Fracture, and Fatigue*. Fourth. Pearson Education Limited, Harlow, Essex, England, 2013.

[17] S. M. Russ, A. H. Rosenberger, J. M. Larsen, and W. S. Johnson. "Fatigue Crack Growth Predictions for Simplified Spectrum Loading: Influence of Major Cycles on Minor-Cycle Damage Rates". *Ageing Mechanisms and Control. Part B - Monitoring and Management of Gas Turbine Fleets for Extended Life and Reduced Costs* (2001). RTO Applied Vehicle Technology Panel Symposium (Manchester, United Kingdom). Published by NATO Research and technology organization (RTO), Neuilly-Sur-Seine Cedex 2003.

[18] J. C. Newman. "A crack opening stress equation for fatigue crack growth". *International Journal of Fracture* 24.4 (1984), R131–R135. ISSN: 0376-9429.

[19] T. L. Andersson. *Fracture Mechanics - Fundamentals and Applications*. Third. CRC Press Inc. Boca Raton, FL, USA, 2005.

[20] D. S. Dugdale. "Yielding of steel sheets containing slits". *Journal of the Mechanics and Physics of Solids* 8 (2 1960), pp. 100–104.

[21] S. U. Khan, R. C. Alderliesten, J. Schijve, and R. Benedictus. "On the fatigue crack growth prediction under variable amplitude loading". *Computational and experimental analysis of damaged materials* (2007), pp. 77–105.

[22] J. C. Newman. "Prediction of fatigue crack growth under variable amplitude and spectrum loading using a closure model". *NASA Technical Memorandum 81942* (1981).

[23] M. Skorupa, T. Machniewicz, J. Schijve, and A. Skorupa. "Application of the strip-yield model from the NASGRO software to predict fatigue crack growth in aluminium alloys under constant and variable amplitude loading". *Engineering Fracture Mechanics* 74.3 (2007), pp. 291 –313.

[24] B. Ziegler, Y. Yamada, and J. C. Newman. “Application of a strip-yield model to predict crack growth under variable-amplitude and spectrum loading - Part 2: Middle-crack-tension specimens”. *Engineering Fracture Mechanics* 78.14 (2011), pp. 2609 –2619.
[25] R. Johansson. *Test specimen - surface crack tension*. GKN Internal Specification, VAC 182395. 1998.
[26] T. Hansson. *Private communication with responsible for RAMGT testing*. GKN Aerospace Engine Systems, Trollhättan, Sweden. 2014.
[27] H. Backström. *Methodinstruktion - Instrumentering av Kb-provstav*. GKN Internal Report (Avdelningsinstruktion 9652-833), Trollhättan, Sweden. 2002.
[28] T. Have. “European Approaches in Standard Spectrum Development”. *Development of Fatigue Loading Spectra*. 1989. ISBN: 0-8031-1185-1.
[29] J. C. Newman. *Private communication via Magnus Andersson*. Mississippi state university, Starkville. 2013.
[30] J. C. Newman. “FASTRAN-II - A fatigue crack growth structural analysis program”. *NASA Technical Memorandum 104159* (1992).
[31] J. Olsson. *Private communication*. GKN Aerospace Engine Systems, Trollhättan. 2014.

Appendices

A Evaluation of risks when using the NASGRO software

This appendix will describe potential issues with the used version of NASGRO, discovered throughout the work with this thesis.

A.1 Difference in SIF solution between crack cases

In the late stages of the thesis, it turned out that different crack cases, setup to be identical, gave different stress intensity factor solutions. The herin described differences are those relevant to the two crack cases currently used to analyze the fan module; SC17 and CC09. The surface crack cases analyzed are SC01, SC02,

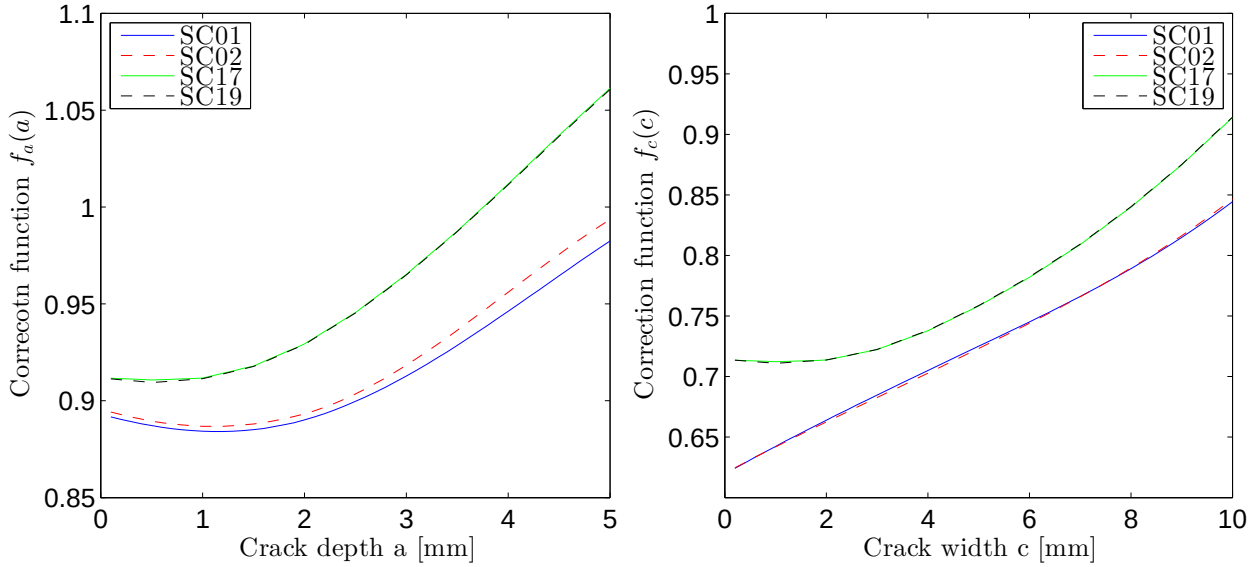

Figure A.1: *Difference in SIF solution for different surface crack cases analyzing equal geometry*

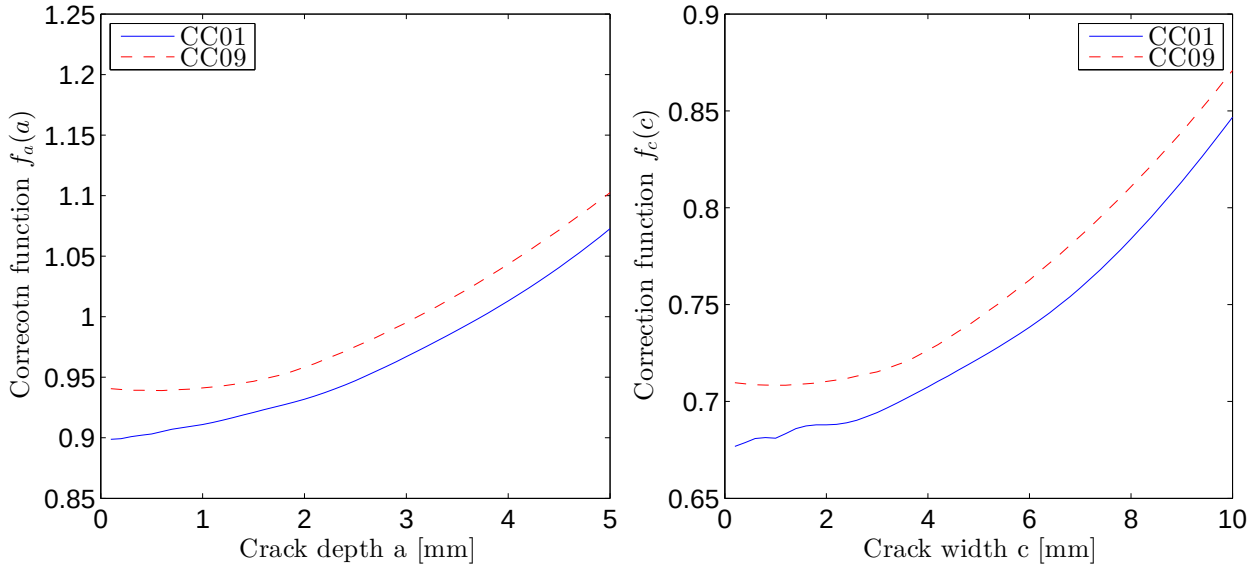

Figure A.2: *Difference in SIF solution for different corner crack cases analyzing equal geometry*

SC17 and SC19 which are increasingly more general compared to each other. SC01 is a centralized surface crack with tension or bending loads. SC02 expands this to employ a weight function allowing the user to input an arbitrary stress field varying throughout the thickness. SC17 allows for off-center cracks in addition, while SC19 can handle a 2-dimensional stress field. The analysis is of a centralized surface crack subjected to pure tension, with twice the half width (c) compared to depth, $a/c = 0.5$. The structure has a width of 100 mm and thickness 10 mm. a goes from 0.1 mm to 5 mm. The geometric correction factor f is such that $K = Sf\sqrt{\pi a}$ and depends on geometry and loading type only. In figure A.1 this correction factor has been plotted against the crack depth or width for each crack case.

As it is clear from the plots, SC01 and SC02 gives lower values than SC17 and SC19, thus the later cases are conservative. There are also small differences between SC01 and SC02, particularly on the a-front, but difference to the two other cases is much greater. In the crack growth relation the SIF range is taken to the power of n (approximately 3), which amplifies these differences.

Similar issues are found between the corner crack cases CC01 and CC09, where CC09 allows for a user defined stress field while CC01 only accepts tension or bending loads. The dimensions for this analysis are equal to those of the surface cracks, using the NASGRO definitions for a and c. The correction functions for each crack front are given in figure A.2.

A.2 Difference in treatment of α in the Strip Yield model between crack cases

As noted in the theory section, the description given in the main reference manual of NASGRO is not always consistent with the behavior of the program in some simulations. In appendix V in the NASGRO manual rules for the plastic constraint coefficient is given. It is unclear if these override the values described in the main reference manual or not. Here, different constraint factors are defined for different crack tip locations. Interior crack tips, such as the depth in surface cracks, are assumed to be under plane strain conditions and $\alpha = 2.55$. Surface crack tips, such as in corner cracks or the width in surface cracks are under plane stress conditions and $\alpha = 1.15$. For through cracks it is here given a relation dependent on the plastic zone size relative thickness based on the maximum stress intensity, $K_{\max}$. From this description one would expect that

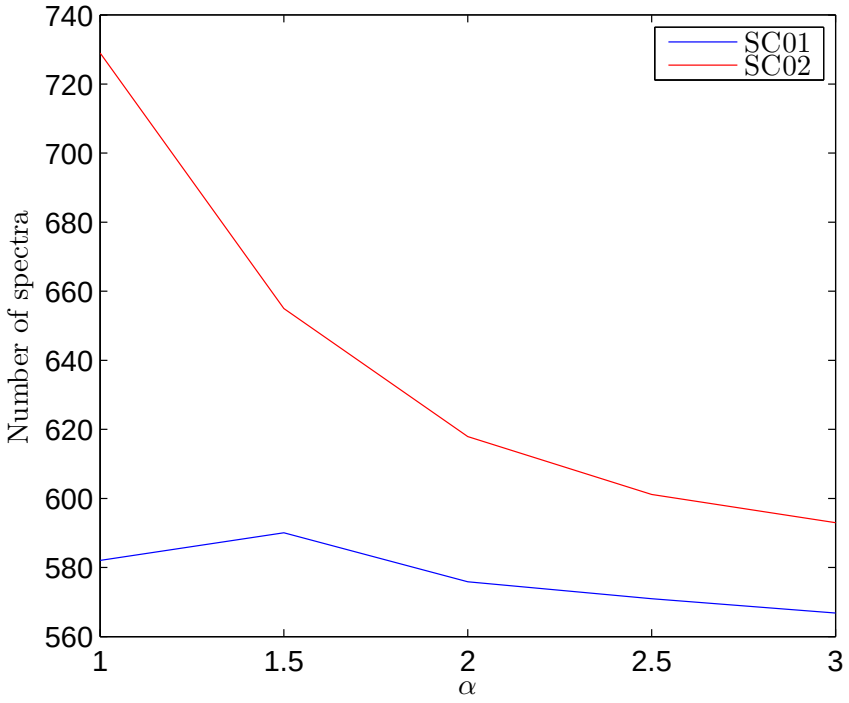

Figure A.3: *Number of spectra to experiment end crack depth variance with α for different crack cases*

the user chosen α will have no effect on any crack case, but as seen this is not the case. Combining with the description in the main reference manual, regarding default values for constraint factor under plane stress and strain, it seems that the user can set the value for plane strain. In that case one would expect that the user choice of α would be neglected in corner crack cases, but have an effect in surface crack cases. Analyzing the spectrum test described in this thesis using both crack case SC01 and SC02, with equivalent inputs, revealed that these treat α differently. In figure A.3 it is clear that the SC02 crack case is much more dependent on α than SC01. These differences are troublesome, particularly since the material data fit, and thus α, has been determined using SC01 while the real analysis use SC02. It is unknown exactly what is different between the crack cases, but at the time of writing the author is waiting for a reply from the NASGRO development team. In the corner crack case it turns out that CC09 is completely unaffected by the user choice of α, while CC01 does depend on α. Thus the implementation is clearly different in this case as well, and the Strip Yield model should be used with caution.

A.3 Corrections for different amount of yielding

In FASTRAN-II Newman added the option of adding a yield correction to the crack length, based on one-fourth of the static plastic zone size calculated using the original Strip Yield model. Based on the experienced gain in this thesis, it is clear that the Strip Yield model does respond to variations on the stress level similarly to what could be expected from such a plastic size zone correction. This type of correction has been assumed, but there is no clear documentation of how it is implemented in NASGRO. To demonstrate the effect of different amounts of yielding, figure A.4 shows the crack growth for the spectrum tests at different flow stress. Thus the applied load remains constant and thereby the LEFM calculated ΔK is constant. It is clear that lowering the flow stress, thus increasing the size of the plastic zone, increase the crack growth rate. If there were no correction due to more yielding, then one would expect a larger yield zone to cause more retardation. This effect is seen when altering α which when changed alter the effective yield limit in tension proportionally. When altering the yield limit directly, the yield zone in compression is also altered which will reduce the retardation effect. Even so, one would not expect so much faster crack growth rate due to this since the tensile plastic zone is increased equivalently. Thus it is the assumption that the Strip Yield model in NASGRO have some

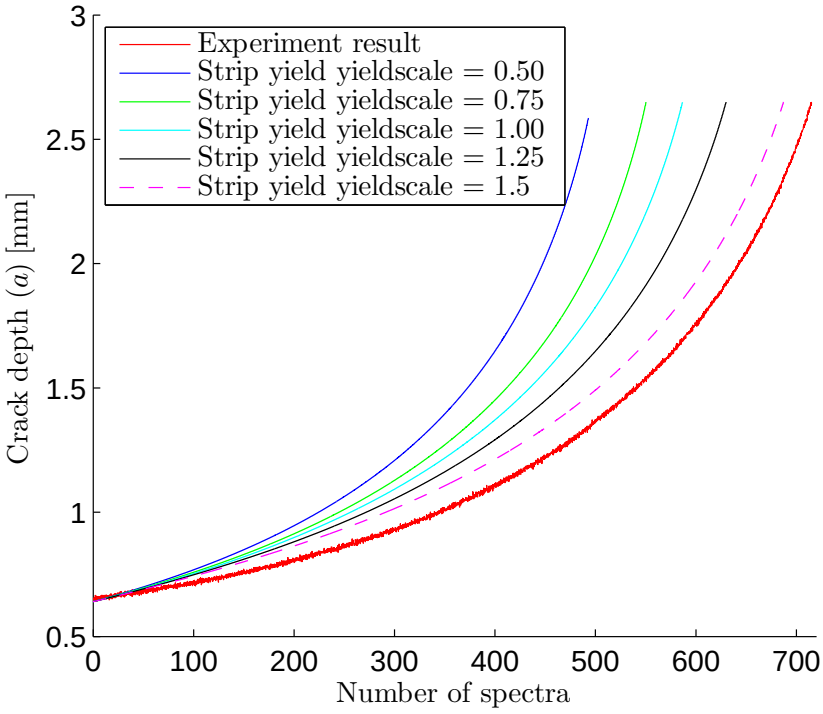

Figure A.4: *Effect of altering flow stress with different scale factors on crack growth rates*

form of compensation in SIF from the size of the yield zone. Since the NASGRO manual claims that the NASGRO implementation of the Strip Yield model is very similar to FASTRAN, it is a reasonable assumption that this phenomenon is treated equally. Questions to the NASGRO development regarding this have been sent, and until it is known exactly how the yield zone size affects the crack growth calculations caution should be exercised when relying on the Strip Yield model to compensate for different stress levels.